Agricultural and Forest Meteorology 359 (2024) 110288

Contents lists available at ScienceDirect

Agricultural and Forest Meteorology

journal homepage: www.elsevier.com/locate/agrformet

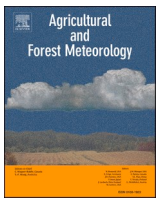

Analysis of scale-dependent spatial correlations of actual evapotranspiration measured by lysimeters

Xiao Lu [a,b,*], Jannis Groh [a,c,d], Alexander Graf [a], Thomas Pütz [a], Katrin Schneider [e], Bingcheng Si [f,g], Harry Vereecken [a], Harrie-Jan Hendricks Franssen [a]

[a] Institute of Bio- and Geosciences - Agrosphere (IBG-3), Forschungszentrum Jülich GmbH, Jülich 52425, Germany
[b] Faculty of Georesources and Materials Engineering, RWTH Aachen University, Aachen 52064, Germany
[c] Institute of Crop Science and Resource Conservations (INRES), Soil Science and Soil Ecology, University of Bonn, Bonn, Germany
[d] Research Area 1 Landscape Functioning, Isotope Biogeochemistry and Gas Fluxes, Leibniz Centre for Agricultural Landscape Research (ZALF), Müncheberg 15374, Germany
[e] Institute of Meteorology and Climate Research (IMK-IFU), Karlsruhe Institute of Technology, Garmisch-Partenkirchen, Germany
[f] College of Resources and Environmental Engineering, Ludong University, Yantai 264025, China
[g] Department of Soil Science, University of Saskatchewan, Saskatoon SK S7N 5A8, Canada

ARTICLE INFO

Keywords:
Evapotranspiration
Weighing lysimeter
Eddy covariance
Spatial correlation
Wavelet coherence

ABSTRACT

Accurate determination of actual evapotranspiration (ETa) is important in various research fields like hydrology, meteorology, ecology and agriculture. *In situ* ETa can be determined using weighing lysimeters and eddy covariance. However, despite being regarded as the most precise *in situ* method for measuring ETa, the information content of lysimeter measurements remains poorly understood. Here we examined the spatial correlations between ETa measured at different locations by lysimeter (ET-LYS) and at different locations by eddy covariance (ET-EC). This was done for the period 2015 - 2020 and the analysis was made for different spatial (range: 0 to 500 km) and temporal scales (range: 1 day to 1 year) using 23 lysimeters and 4 eddy covariance towers. We found that: (a) Same lysimeters at the plot scale show very high correlations of ET-LYS; (b) The Pearson correlation of daily standardized anomalies of ET-LYS between sites exhibit moderate to high correlations and were similar to that of ET-EC, indicating that lysimeter is generally as representative as EC regarding ETa, and can provide certain information at the landscape and larger regional scale. During winter, the spatial correlations for ET-LYS were smaller; (c) Wavelet analysis indicated that temporal correlations in ETa were strongest for distances in time around 12 months (yearly cycle) and less than three months. Spatial correlations were smaller under drought conditions (in the year 2018). Furthermore, combination of multiple ET-LYS from different sites improved the predictability of ET-LYS for another site, suggesting that ET-LYS can be predicted well using ET-LYS from different neighboring sites. Overall, lysimeter measurements can provide information at much larger scales compared to their small measurement area.

1. Introduction

Evapotranspiration (ET) is a central component of the terrestrial water cycle and links the hydrosphere, atmosphere and biosphere (Fisher et al., 2017), which includes evaporation from soil, transpiration by vegetation and evaporation of water on vegetation (Hanson, 1991; Kool et al., 2014). Potential evapotranspiration (ET_0) is the ET amount for a specific reference vegetation if there are no limitations on water availability. Actual evapotranspiration (ETa) refers to the ET which really takes place, affected by possible water scarcity. The precise assessment of ETa is essential for a broad range of scientific disciplines including agricultural water management, drought monitoring as well as sustainable use of water resources (Negm et al., 2017; Awada et al., 2019; Li et al., 2022).

Unfortunately, the accurate determination of ETa remains a challenge, as it is a variable that is difficult to measure and parametrize (Cuxart & Boone, 2020). Typical approaches to determine ETa include *in situ* stations like eddy covariance (EC) stations and lysimeters or estimates via remote sensing. Remote-sensing based ETa estimates, though promising and widespread, have large uncertainties and require ground

* Corresponding author at: Institute of Bio- and Geosciences - Agrosphere (IBG-3), Forschungszentrum Jülich GmbH, Jülich 52425, Germany.
E-mail address: xi.lu@fz-juelich.de (X. Lu).

https://doi.org/10.1016/j.agrformet.2024.110288
Received 13 February 2024; Received in revised form 13 September 2024; Accepted 24 October 2024
Available online 30 October 2024

validation (Mueller et al., 2011; Seneviratne et al., 2012; Tran et al., 2023). Therefore, ground-based observations remain the most established reference measurements (Hirschi et al., 2017). EC is a prevalent micrometeorological technique for ground-based ETa measurements with relative low operational expenses (Ding et al., 2010; Dhungel et al., 2021; Han et al., 2021). An EC system can capture field-scale ETa information within the measurement footprint of the installed EC tower, covering approximately 100 m to few kilometers in radius around the towers (Zhang et al., 2014; Chu et al., 2021; Levy et al., 2022; Zhu et al., 2023), but are subjected to systematic measurement errors (e.g., Wilson et al., 2001; Franssen et al., 2010; Mauder et al., 2020; Zhang et al., 2022) and random measurement errors (Hollinger & Richardson, 2005; Kessomkiat et al., 2013; Post et al., 2015).

Weighing lysimeters are another common ground-based observation technique, and are considered the best mean to directly measure ETa *in situ* (Allen et al., 2011; Schrader et al., 2013; Gebler et al., 2015; Peters et al., 2017; Sánchez et al., 2019). They contain soil columns that are separated from the surrounding soil and can determine the weight of the column gravimetrically. The information on the weight changes can be used to determine the water fluxes across the soil – vegetation – atmosphere interface with high precision (Unold & Fank, 2008). Since the construction of the first weighing lysimeter in Germany in 1902, the technology has improved a lot to assess the changes in the soil water storage of the soil column that fills the lysimeter (Goss & Ehlers, 2009). An example are the lysimeters of the German TERrestrial ENvironmental Observatories (TERENO) SOILCan network which are of high accuracy and high temporal resolution and provide the opportunity for in-depth long-term investigations of the different components of the soil water cycle (Zacharias et al., 2011; Pütz et al., 2016). The ability to successfully quantify small water fluxes such as dew and hoar frost formation as well as nighttime ETa demonstrates the high precision of the lysimeters (Groh et al., 2018; 2019). In addition, Gebler et al. (2015) carried out a study with one lysimeter site of this network to compare ETa estimated by EC and lysimeter. The study illustrated that a lysimeter can measure ETa in a reliable manner and does not suffer from some of the drawbacks of EC systems. Trigo et al. (2018) used the ETa data from the same site for a follow-up period and showed that ETa was underestimated by the EC technique and required a correction factor of 1.15 when compared to ETa data from weighing lysimeters. Similarly, Mauder et al. (2018) took lysimeter measurements at two grassland ecosystems from TERENO-SOILCan as a reference to evaluate the energy balance problem for EC measurements and found EC-based ETa was generally underestimated.

However, weighing lysimeters also have several disadvantages, such as their small footprint (pedon-scale) due to limited surface area and their limitation in quantifying ETa from forested land. A main question is therefore how informative the precise ETa-measurements by weighing lysimeters are. Evett et al. (2012) evaluated several methods for quantifying ETa at different spatial scales with the same soil and crop over one growing season and found that ETa derived from weighing lysimeters sufficiently represents the surrounding field ETa throughout the season. They also pointed out that differences in plant height and width would result in a mismatch between ETa from the lysimeters and the surroundings. Seneviratne et al. (2012) reported that lysimeter measurements are representative of a small catchment (3.31 km^2) although a scale discrepancy existed by comparing 32-year data sets of lysimeter seepage with the discharge from the small catchment. They pointed out that the most significant differences between lysimeter seepage and catchment runoff occurred in March. This variation was likely associated with a greater spatial variability of hydrological processes during that month, which could be attributed to factors such as snowmelt and the initiation of the growing season. For the same research catchment in Switzerland, Hirschi et al. (2017) revealed that the long-term lysimeter measurements corresponded well with catchment water-balance evaluations of ETa. This emphasizes that lysimeter measurements can be representative for the entire catchment, despite the relatively small source areas (typically about 3 m^2) and the diverse land use and topography within the catchment. Teuling (2018) found that ETa from four different lysimeter stations in three countries with contrasting vegetation and climate are in line with ETa estimates from catchment-scale water balance studies. Widmoser and Michel (2021) compared concurrent lysimeter and EC measurements across four grassland sites. In this study, they applied a partial energy closure method to correct EC measurements, wherein they evaluated the correction factor for latent heat flux by regressing the difference between the lysimeter and EC latent heat fluxes and used this weight to correct the EC latent heat flux. In contrast to this, Denager et al. (2020) found a good agreement and no statistical difference between uncorrected ETa measured by EC and ETa estimated by the water balance method where recharge was measured by non-weighable percolation lysimeters. They attributed this agreement to the fact that the spatial scale of the water balance method in this study was compatible with the EC measurement scale. They pointed out that in other studies EC-estimated ETa was always underestimated compared with ETa measured by weighing lysimeters, possibly because weighing lysimeters were not representative for the entire field. In addition, Denager et al. (2022) emphasized again that the total surface area of the lysimeters is quite small compared to the footprint of the EC system. Although these studies point to the fact that lysimeter ETa contain information for larger areas, e.g., they are comparable with measurements within EC footprint or even can be representative for a catchment, this has never been analyzed in a systematic manner.

The core objective of this study is to provide systematic evidence that lysimeter ETa measurements provide, despite their small surface area, representative information for larger areas such as the plot scale, landscape scale (10 ~ 50 km) and larger regional scale (500 km). To this end, we analyzed daily ETa measurements by a total of 23 lysimeters at four study sites across Germany (separation distances from 0 to 500 km) for six consecutive years (2015 to 2020). As EC estimates at the field scale, we compare spatial correlations of standardized anomalies of ETa between different lysimeters with spatial correlations of standardized anomalies of ETa between different EC stations, at the same measurement sites. If the lysimeter ETa is more affected by random fluctuations (i.e., measurement errors and small scale variability which cannot be attributed to any specific pattern or trend), related to the small footprint, we would expect smaller spatial correlations of lysimeter ETa between the measurement sites than spatial correlations of EC derived ETa. The spatial correlations are analyzed further, also on different temporal scales, with wavelet transform coherence (WTC) analysis, which overcomes the limitations of Fourier transform in analyzing nonstationary time series, not only to identify the scale and frequency of temporal patterns in a time series, but also to identify coherence between two time series at different scales and frequencies (Bravo et al., 2020). Compared to a single correlation coefficient, WTC allows to identify how correlations vary between years and seasons. Furthermore, measuring the correlation of two ETa time series will not fully capture all the features of ETa processes given the complex space-time links between climate, soil and vegetation (Rodriguez-Iturbe, 2000; Kim et al., 2022). Thus, it is essential to study multiple ETa time series at multiple space-time domains to better reveal the relationship of ETa among different locations. The multiple wavelet coherence (MWC) approach has been shown to be suitable to untangle a range of multivariate relationships in the field of geosciences (Hu & Si, 2016; Hu et al., 2017; Su et al., 2019; Cheng et al., 2021). MWC is therefore conducive to proper characterization of the temporal scale specific multivariate relationships between ETa measurements under different climate, soil and vegetation conditions. A good understanding of these relationships is important for optimizing the prediction of ETa for a given site using the measurements at other sites, and also for determining the number of lysimeter needed to be representative for a given spatial scale and thus optimizing the design of a lysimeter network.

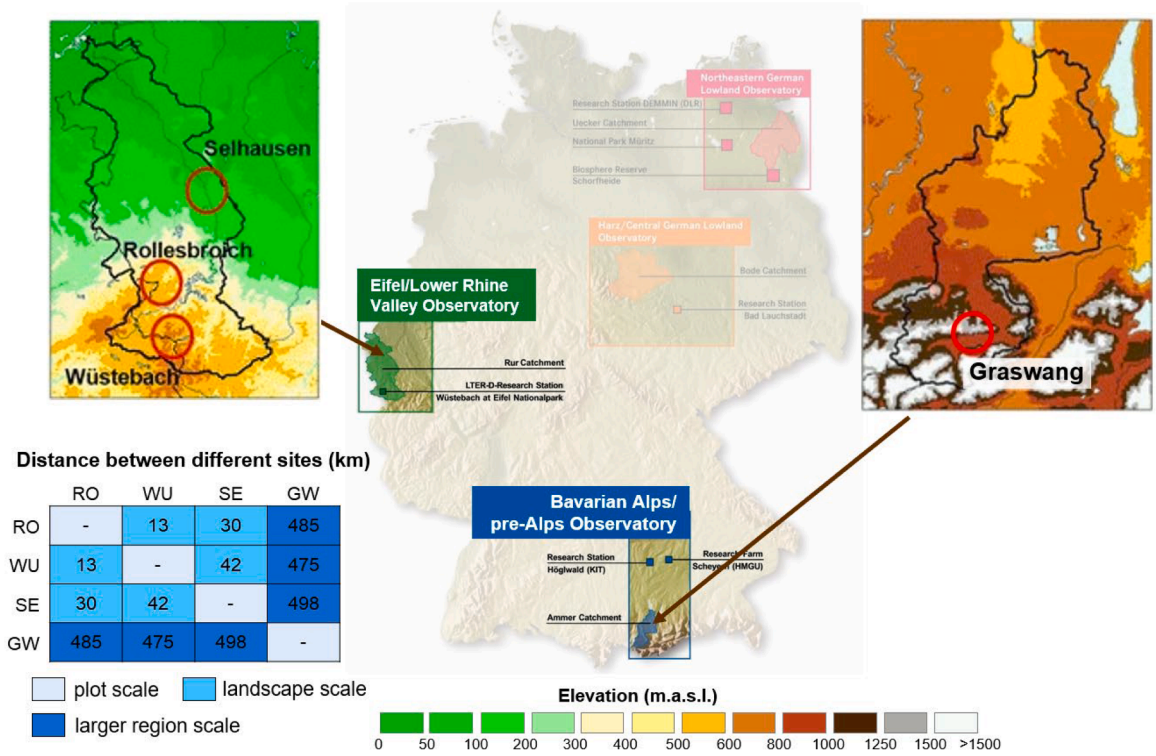

Fig. 1. Location of TERENO observatories over Germany and locations of the four study sites (marked by red circle), as well as distances (in km) between different sites (three different shades of blue are used to indicate different spatial scales; modified from Pütz et al., 2016). RO: Rollesbroich, WU: Wüstebach, SE: Selhausen, GW: Graswang.

Table 1
Specifications of the four lysimeter (LYS) sites used for the analyses in this paper including location, number of individual lysimeters, soil information and land use.

Site	location	Elevation (m a. s.l.)	Abbr.	No. of LYS	LYS name	Soil origin	Soil location	Soil texture*	Vegetation (LYS)	Ecosystem (EC)
SE	50°52′8″N 6°26′59″E	104	SEse	3	Se_Y_032, 033, 034	SE	SE	silty loam	crop	crop
			SEro	3	Se_Y_021, 025, 026	RO	SE	clay loam	grass	
			SEwu	3	Se_Y_022, 023, 024	WU	SE	clay loam	grass	
RO	50°37′18″N 6°18′15″E	515	RO	6	Ro_Y_011, 012, 013, 014, 015, 016	RO	RO	clay loam	grass	grass
WU	50°30′10″N 6°19′42″E	625	WU	6	Wu_Y_011,012, 013, 014, 015, 016,	WU	WU	clay loam	grass	forest
GW	47°34′15″N 11°01′57″E	864	GW	2	GW_1_3, 1_5	GW	GW	clay	grass	grass

* Classification of soil texture is based on the texture triangle developed by the USDA (United States Department of Agriculture).

2. Materials and methods

2.1. Study sites

The four study sites are part of the TERENO network in Germany. Fig. 1 displays the location of the sites, together with the spatial distances between the sites. Table 1 provides further information on the sites and the different lysimeters used from the sites. The Selhausen (SE), Rollesbroich (RO) and Wüstebach (WU) sites belong to the Eifel/Lower Rhine Valley Observatory which is located along the western border of Germany and covers a total area of 2354 km^2 (Bogena et al., 2018). Among these three sites, the Selhausen site (SE) has the least amount of mean annual precipitation (700 mm/y) and the highest mean annual air temperature (10 °C) for the period from 1961 to 2014. The crops on this arable land are dominated by winter cereals (mainly winter wheat), sugar beet and maize. The prevalent soils are (gleyic) cambisol and (gleyic) luvisol, both of which are characterized as silty loam textures (Korres et al., 2015). The grassland site RO has a mean annual air temperature of 7.7 °C and a mean annual precipitation of 1033 mm/y for the period 1981–2001. Stagnosol is the major soil type in the northern part, whereas cambisol (gleyic) dominates the soil in the southern part of the site. The plant community is mainly comprised of *Lolium perenne* and *Trifolium repens* (Forstner et al., 2021). During the study period, the vegetation on the lysimeter and the surrounding field is subjected to extensive management, including 3~4 cuts and 2~3 liquid manure applications (~1.6 L/m^2) per growing season following the local agricultural management (Groh et al., 2019). The mean annual air temperature and precipitation for the Wüstebach site (WU) are 8.2 °C and 1310 mm/y (1991 to 2013), respectively. The vegetation at this forest site is dominated by spruce trees (Norway spruce, *Picea abies* L.) and amended by Sitka spruce (*Picea sitchensis*). The vegetation on and around the lysimeter corresponds to a forest meadow and the plant community consists of *Agrostis capillaris* and *Galium saxatile* (Groh et al., 2019). On the hillslopes the major soils are cambisols and planosols, whereas in the riparian zone the main soils are gleysols and histosols. The soil texture is clay loam with coarse material inclusions. Graswang

(GW) is approximately 500 km away from the aforementioned three sites and belongs to the Bavarian Alps/pre-Alps observatory (Kiese et al., 2018). This site is situated in grassland ecosystems primarily used for fodder and hay production in the Ammer catchment of southern Germany (Zeeman et al., 2017). It has a temperate oceanic climate with a mean annual precipitation of 1347 mm/y and a mean annual temperature of 6.9 °C (2012 to 2018). The soil in GW is classified as fluvic calcaric cambisol and the soil texture is clay (Fu et al., 2017). The vegetation is composed of grasses and herbs, with a small proportion of clover. Main species are *Festuca pratensis, Poa pratensis, Prunella vulgaris, Plantago lanceolate, Knautia arvensis and Pimpinella major* (Fu et al., 2019). The site GW underwent extensive management consisting of 3 cuts and 1 manure application per year following local farmers' practices (Fu et al., 2019).

2.2. Lysimeters set up

At each site of the TERENO-SOILCan lysimeter network, at least a set of six individual lysimeters (UMS GmbH, Munich, Germany) with a surface area of 1.0 m^2 and a depth of 1.5 m are arranged in a standardized hexagonal design. The distance between the lysimeters at the same site is only a few meters (about 3 - 6 m). The lysimeter stations have equal experimental and monitoring conditions. The highly precise (resolution of 10 g) and resolved (1 min measurements) lysimeters have a dynamic control bottom boundary. Here, differences between matric potential measured in the field at 1.4 m soil depth and in the lysimeter at 1.4 m depth are minimized based on an adjustable algorithm that controls the water flux rate and direction via a bi-directional pumping system (Pütz et al. 2016). This dynamic bottom boundary control ensures that the soil water dynamics of the lysimeter match field conditions regarding their water flux direction and rate (Groh et al., 2016). Further technical specifications of the lysimeter used in this study are found in Pütz et al. (2016).

In our study, we used a total of 23 high-precision weighing lysimeters. The lysimeters from RO, WU and GW always contain local soil, while for SE there are three lysimeters with local soil, three lysimeters with soil from WU and three lysimeters with soil from RO. In detail, nine lysimeters were excavated at RO, whereby six of them remained in RO and the other three (Se_Y_021, Se_Y_025, and Se_Y_026) were transferred along an altitudinal gradient to SE in winter 2010. These soils are denoted by "SEro" in this paper. At WU, similar to RO, six out of nine lysimeters are located at WU, and the other three (Se_Y_022, Se_Y_023, and Se_Y_024) were transferred to SE and are referred as "SEwu". Three lysimeters in SE (Se_Y_032, Se_Y_033, and Se_Y_034) are filled monolithically with local soil and were managed with a cereal crop rotation and named as "SEse" in this study. At GW, two well-managed lysimeters (GW_1_3 and GW_1_5) were used for this work. They both contain the local intact soil monoliths and are subject to the same extensive management as the surrounding field.

2.3. Lysimeter data

Lysimeter raw data were recorded at 1 min intervals, which allows to directly determine precipitation (P) including non-rainfall water (i.e., dew, rime, and fog), and ETa from lysimeter weight changes using the soil water balance equation (Schrader et al., 2013). This soil water balance equation takes weight changes related to water fluxes across the lysimeter bottom (percolation, capillary rise) into account. In this study, we didn't separate between rain and non-rainfall events, thus P stands for all incoming atmospheric moisture which also includes water inputs from non-rainfall events. The amount of P is determined from the increase of lysimeter weight after correcting the weight changes for the water fluxes across the lysimeter bottom. The procedure assumes that only P or ETa can occur within a 1 min period.

Lysimeter data are prone to wind or other external disturbances. Thus, lysimeter weight data were processed by a pre- and post-processing routine to reduce external errors and noise to the determination and separation of water fluxes over the land surface. In a first step, the raw lysimeter data from 2015 until 2020 underwent a manual and automatic plausibility check (Schneider et al., 2021). During the automated data control process, outliers or other disturbances in the lysimeter and tank weight data were eliminated. In a second step, the adaptive window and threshold filter was applied (AWAT; Peters et al., 2014, 2017) to reduce the impact from external errors and noise on the determination of P and ETa. Typically, the high frequency of lysimeter weight measurements in combination with the AWAT-filter allowed to precisely estimate ETa or P rates, including small water fluxes from dew formation, soil water vapor adsorption, or nighttime ETa (Groh et al., 2019; Kohfahl et al., 2019; Paulus et al., 2022). In the next step, the lysimeter ETa data (ET-LYS) were aggregated to hourly values. Missing hourly values were gap-filled using linear regression with parallel ETa values from other available lysimeters (same site and same soil) or the potential ET (ET_0) for a grass reference vegetation with an albedo of 0.23. The hourly ET_0 is calculated with the FAO Penman-Monteith equation (Allen et al., 2006):

$$ET_0 = \frac{0.408\Delta(R_n - G) + \gamma \frac{37}{T_h+273} u_2 (e^o(T_h) - e_a)}{\Delta + \gamma(1 + C_d u_2)} \quad (1)$$

where Δ is the slope of the vapor pressure curve (kPa $°C^{-1}$), R_n is net radiation at the surface (MJ m^{-2} h^{-1}), G is soil heat flux density (MJ m^{-2} h^{-1}), T_h is mean hourly air temperature at 2 m height (°C), $e^o(T_h)$ is hourly saturation vapor pressure (kPa), e_a is hourly actual vapor pressure (kPa), γ is psychrometric constant (kPa $°C^{-1}$), C_d is the coefficient set to 0.24 s m^{-1} when $R_n > 0$ and 0.96 s m^{-1} when $R_n < 0$, and u_2 is wind speed at 2 m height (m s^{-1}).

However, lysimeter data during snow cover and freezing conditions are often prone to larger errors due to the influence of snow bridges and ice formation (Schnepper et al., 2023). Thus, longer gaps during winter and spring (December to March, Table S3) due to snow or ice cover on the top of the lysimeters existed at the alpine site GW. We used hourly $ET_{0,snow}$ to replace the missing hourly values for these gaps. $ET_{0,snow}$ is the potential ET calculated with the actual albedo measurements instead of the albedo for grass (0.23). Actual albedo was measured using the sensor CNR4 (Kipp & Zonen, Delft, Netherlands) at the height of 1.9 m at the GW site. Finally, the hourly data were aggregated to daily values.

2.4. Eddy covariance data

Eddy-covariance measurements are conducted near each lysimeter station. The equipment used at the different EC-stations is basically identical. The EC instrumentation consists of a CSAT-3 sonic anemometer (Campbell Scientific, Inc., Logan, USA) to measure wind for all three dimensions, and an LI7500 open-path gas analyzer (LI-COR Inc., Lincoln, NE, USA) for acquisition of H_2O and CO_2 contents of the air. Along with the anemometer and gas analyzer, a four-component net radiometer (Eifel: NR01, Hukseflux Thermal Sensors, Delft, Netherlands; Pre-Alpine: CNR4, Kipp & Zonen, Delft, Netherlands) and soil heat flux plates (HFP01-SC, Hukseflux Thermal Sensors, Delft, Netherlands) are installed to measure radiative fluxes and ground heat flux. Air temperature and humidity are measured by HMP45 (Vaisala Inc., Helsinki, Finland). More information about the EC station can be found for the individual sites in Bogena et al. (2018) and Kiese et al. (2018).

The EC raw data were obtained at a frequency of 20 Hz, followed by the aggregation of fluxes to 30 min intervals. The EC data calculation and quality assurance were conducted in accordance with the standardized strategy proposed by Mauder et al. (2013) using the TK3 software package (Mauder & Foken, 2011). Only flux data with quality flags 0 and 1 were used in this study; other poor quality data were excluded. To fill the gaps, a zero-intercept linear regression approach between ETa and the predictor ET_0 with a flexible time window was applied according to Graf et al. (2014). The window length starts at a

minimum of 60 days and then increases by 1 h increments to find the minimum root mean square error (RMSE). We continued to increase the window length until either (1) the RMSE started to rise as the time window expanded or (2) the maximum allowable window length of 120 days was achieved. Eventually, the regression coefficient (the slope of ETa versus ET_0 values) associated with the chosen time window was used to fill the missing values. More specifications can be found in Graf et al. (2014).

We mainly focused on the estimation of ETa without correction of the energy balance deficit. However, energy imbalance is a common issue at almost every EC site, where the sum of the turbulent fluxes (sensible plus latent heat flux) is generally less than the measured available energy (net radiation minus ground heat flux) (Twine et al., 2000; Foken et al., 2011). To address this discrepancy, the turbulent fluxes can be recalculated using the Bowen-ratio forced closure method. In this study, the energy balance deficit (EBD) was determined on a daily scale:

$$\mathrm{EBD} = \mathrm{R_n} - (G + \mathrm{LE} + H) \tag{2}$$

where R_n is net radiation (W m^{-2}), G is ground heat flux (W m^{-2}), LE is latent heat flux (W m^{-2}), and H is sensible heat flux (W m^{-2}).

The Bowen ratio (β) is defined as:

$$\beta = \frac{\mathrm{H}}{\mathrm{LE}} \tag{3}$$

The energy-balance-corrected latent heat flux (LE_c) was then determined by redistributing the latent heat according to the calculated Bowen ratio:

$$\mathrm{LE_c} = \mathrm{LE} + \mathrm{EBD}\left(1 + \frac{1}{\beta}\right) \tag{4}$$

Both uncorrected and corrected ETa measurements from EC (ET-EC and ET-ECc, respectively) were used in this study to assess whether the closure of the energy balance from EC measurements affects the correlations of ETa between sites.

2.5. Pearson correlation coefficient of standardized anomalies of ETa

Pearson correlation coefficient (PCC) is a classic metrics of the strength and direction of a linear relationship between two variables. For a sample size larger than 30, the absolute values of PCC ranging between 0 and 0.1 indicate no correlation, 0.1–0.3 small correlation, 0.3–0.5 moderate correlation and 0.5–1.0 strong correlation (Cohen, 1988; Fraenkel & Wallen, 1990).

If ETa values are known over a long time period, long term averages of ETa can be calculated, and anomalies can be deduced from this. For example, it is expected that under conditions of sufficient water supply and higher availability of energy than normal (sunny and warm weather conditions) ETa will show a positive anomaly, whereas under conditions of very low soil moisture content, ETa will be below normal. The anomaly for a given period is calculated by comparing with the historical mean for the same period so that surplus or deficit can be calculated (Tadesse et al., 2015). ETa anomaly (ΔET_a) is defined as ETa for the day i ($ET_{a,i}$) minus the long-term average ETa for that day ($\overline{ET_{a,i}}$):

$$\Delta \mathrm{ET}_a = ET_{a,i} - \overline{ET_{a,i}} \tag{5}$$

ΔET_a is calculated on a daily basis. As the time series of ETa in this study are still relatively short, average ETa shows still considerable day-to-day variations. Therefore, the yearly cycle of average daily ETa is smoothed with help of a fourth order polynomial regression. For the subsequent statistical analysis of the ETa, it is also important to standardize for time dependent standard deviation (e.g., the standard deviation of ETa is in general smaller in winter than in summer). SA_{ET_a} were calculated as follow:

$$SA_{ET_a} = \frac{\Delta \mathrm{ET}_a}{\sigma_{\mathrm{ET}_a,\ \mathrm{i}}} \tag{6}$$

where $\sigma_{ET_a,\ i}$ is the long-term standard deviation of daily ETa for that day of the year, which is obtained from a fourth order polynomial regression. Standardized anomalies eliminate the role of seasonality (Grumm & Hart, 2001). The SA_{ET_a} are then subjected to statistical analysis focusing on spatial correlations between different sites evaluated by PCC. This calculation procedure was followed for ET-LYS, ET-EC and ET-ECc.

2.6. Wavelet analysis

The behavior of ETa can differ across various temporal scales. The correlation for ETa between sites can be positive at some temporal scales, whereas at other scales it can be negative. In order to analyze the correlations into time-frequency domain as well as for lagged responses, wavelet transform coherence (WTC) was employed. Furthermore, multivariate relationships of ETa at multiple scales are also an interesting investigation for our better understanding of ETa measurements and are important to improve the accuracy of ETa predictions for a specific location based on data from different locations. With the combination of different ETa time series, more climate conditions, vegetation types and soil types are taken into consideration. We applied multiple wavelet coherence (MWC) which is able to disentangle a range of multivariate relationships.

2.6.1. Continuous wavelet transform

Continuous wavelet transform (CWT) analyzes a time series in time-frequency domain (Torrence & Compo, 1998; Grinsted et al., 2004). Before WTC and MWC can be calculated, it is essential to first compute the CWT.

For a time series X of length N (X_n, $n = 1, 2, \ldots, N$) with uniform sample spacing δt (one day in this study), the CWT can be computed as:

$$W_n^X(s) = \sum_{n'=1}^{N} x_{n'} c_s \psi_0\left(\frac{(n'-n)\delta t}{s}\right) \tag{7}$$

where n is the localized time index, n' is the time variable, N is the number of points in the time series, s is the wavelet scale, $c_s = \sqrt{\frac{\delta t}{s}}$ is the normalization factor and $\psi_0(\ )$ is the mother wavelet function. In this study, the Morlet wavelet was selected as the mother wavelet which has been widely used in hydrometeorological studies (Labat, 2005; Charlier et al., 2015; Su et al., 2019; Cheng et al., 2021; Wu et al., 2021). The Morlet wavelet function is expressed as $\psi_0(\eta) = \pi^{-1/4} e^{i\omega_0\eta} e^{-\eta^2/2}$, where i is the imaginary operator ($i = \sqrt{-1}$), η is the dimensionless time and ω_0 is the dimensionless frequency localization. The value of ω_0 is commonly recommended as 6 which can provide a good balance between time and frequency localization for feature extraction purposes (Grinsted et al., 2004).

2.6.2. Wavelet transform coherence

WTC is a correlation coefficient in the time - frequency space and can quantify the intensity of linear relationship between two time series. Given time series X and Y, with wavelet transforms $W_n^X(s)$ and $W_n^Y(s)$, the WTC between X and Y can be expressed as:

$$R_n^2(s) = \frac{\left|S\left(s^{-1} W_n^{XY}(s)\right)\right|^2}{S\left(s^{-1}\left|W_n^X(s)\right|^2\right) \cdot S\left(s^{-1}\left|W_n^Y(s)\right|^2\right)} \tag{8}$$

where $W_n^{XY} = W_n^{XY}(s) \cdot W_n^{XY} *(s)$ is the cross-wavelet spectrum, * denotes the complex conjugate and S is a smoothing operator (for detailed information, see Torrence & Compo, 1998). The value of $R_n^2(s)$ ranges from 0 to 1, with 0 indicating no correlation and 1 indicating the perfect linear relationship between the two time series at the given frequency

Table 2
Yearly sums of ET_0, ET-LYS, ET-EC and ET-ECc at different sites. "Gap-filled ETa [%]" denotes the percentage of hourly ETa which were gap-filled. Here, yearly ET-LYS is the mean of multiple lysimeters at the same site. The standard deviations between the lysimeters are presented in parentheses.

Site	Year	2015	2016	2017	2018	2019	2020	Mean
RO	ET_0 [mm]	673.5	630.7	655.3	737.1	689.0	763.9	691.6
	ET-LYS [mm]	684.3 (±20.4)	642.1 (±18.3)	658.9 (±27.6)	658.3 (±34.4)	708.8 (±35.8)	708.2 (±23.9)	676.8 (±19.0)
	ET-EC [mm]	535.8	481.4	540.9	550.1	516.4	553.9	529.7
	$ET\text{-}EC_c$ [mm]	619.5	614.8	652.2	661.1	611.6	664.6	637.3
	Gap-filled ET-LYS [%]	16.2 (±2.34)	11.4 (±0.63)	12.7 (±0.41)	17.5 (±0.35)	18.5 (±9.80)	7.8 (±0.91)	14.0 (±4.11)
	Gap-filled ET-EC [%]	30.4	32.8	33.2	26.6	29.2	27.3	29.90
WU	ET_0 [mm]	628.7	592.9	598.2	691.8	648.2	694.1	642.3
	ET-LYS [mm]	469.9 (±26.6)	399.4 (±35.1)	389.9 (±29.7)	428.0 (±27.4)	376.1 (±23.8)	373.3 (±27.9)	406.1 (±25.8)
	ET-EC [mm]	507.0	543.1	550.4	528.2	516.9	532.1	529.6
	$ET\text{-}EC_c$ [mm]	553.8	581.8	557.0	577.9	555.5	584.4	568.4
	Gap-filled ET-LYS [%]	12.1 (±0.74)	16.5 (±0.83)	17.2 (±0.86)	18.8 (±1.44)	16.4 (±1.07)	13.0 (±1.99)	15.7 (±1.15)
	Gap-filled ET-EC [%]	51.5	51.1	64.2	65.3	50.9	47.9	55.2
SE	ET_0 (mm)	741.1	690.4	709.6	800.7	766.6	828.6	756.2
	ET-LYS(SEse) [mm]	733.4 (±36.6)	506.0 (±14.1)	570.4 (±46.9)	471.2 (±11.4)	533.5 (±34.1)	480.7 (±23.0)	549.2 (±9.9)
	ET-LYS(SEro) [mm]	838.0 (±23.9)	694.0 (±43.6)	681.5 (±30.1)	592.2 (±16.5)	731.5 (±33.6)	672.5 (±5.5)	701.6 (±13.2)
	ET-LYS(SEwu) [mm]	709.8 (±65.3)	611.4 (±63.8)	563.1 (±39.7)	477.1 (±19.9)	486.6 (±37.9)	490.3 (±36.3)	556.4 (±31.9)
	ET-EC [mm]	586.2	496.4	538.7	449.1	522.1	487.2	513.3
	$ET\text{-}EC_c$ [mm]	683.6	609.1	639.1	534.3	664.6	568.5	616.5
	Gap-filled ET-LYS (SEse) [%]	7.9 (±1.89)	5.5 (±0.99)	6.3 (±2.98)	5.3 (±0.58)	4.1 (±0.54)	2.9 (±0.90)	5.3 (±1.71)
	Gap-filled ET-LYS (SEro) [%]	12.4 (±4.49)	8.2 (±1.42)	5.8 (±0.40)	4.1 (±0.87)	8.2 (±0.46)	4.3 (±0.55)	7.2 (±3.15)
	Gap-filled ET-LYS (SEwu) [%]	12.7 (±6.65)	9.0 (±0.83)	5.8 (±1.18)	6.9 (±1.13)	12.4 (±2.56)	7.4 (±0.74)	9.0 (±2.89)
	Gap-filled ET-EC [%]	19.5	20.4	22.3	18.6	18.2	26.8	21.0
GW	ET_0 [mm]	674.2	623.7	666.1	705.8	681.5	666.7	669.7
	ET-LYS [mm]	637.5 (±2.9)	585.7 (±37.7)	659.2 (±50.0)	663.1 (±28.9)	665.8 (±54.8)	697.1 (±15.1)	651.4 (±31.6)
	ET-EC [mm]	462.6	446.3	507.0	492.3	459.6	465.6	472.2
	$ET\text{-}EC_c$ [mm]	572.4	506.4	546.2	556.1	474.0	495.9	525.2
	Gap-filled ET-LYS [%]	49.9 (±0.6)	41.5 (±0.6)	43.1 (±3.0)	45.2 (±1.4)	54.1 (±3.0)	59.7 (±1.7)	48.9 (±7.0)
	Gap-filled ET-EC [%]	39.3	39.2	38.4	57.3	30.4	30.7	39.2

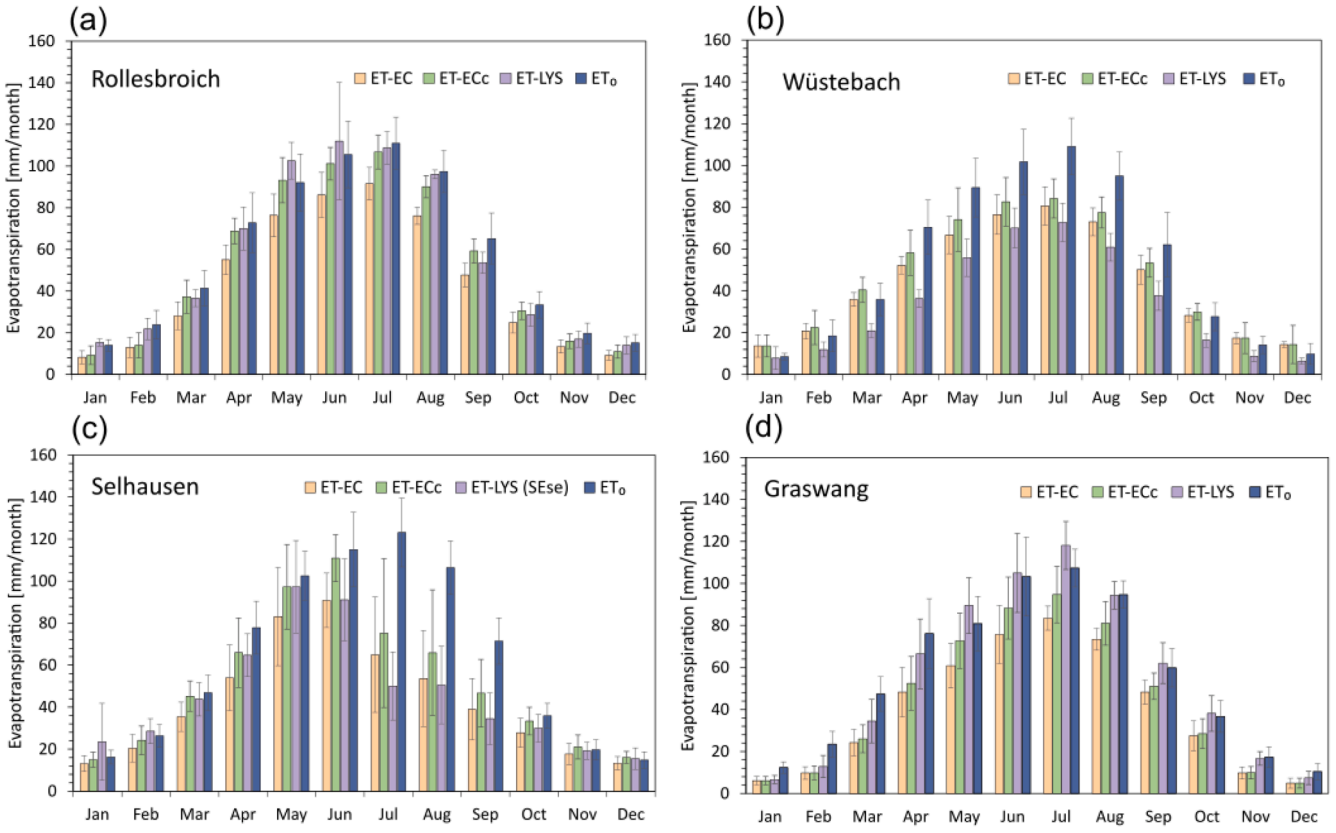

Fig. 2. Average monthly cumulative ET-LYS, ET-EC, ET-ECc and ET_0 at different sites, calculated over the period 2015–2020. Error bars denote the standard deviations of monthly ET, calculated over the years.

Table 3
Average Pearson correlation coefficient (PCC) of SAET-LYS, calculated between different pairs of lysimeters at the same site for the period 2015–2020. Stdv denotes the standard deviation of correlations.

	RO	WU	SEro	SEwu	SEse	GW
PCC	0.96	0.94	0.92	0.91	0.94	0.95
Stdv	±0.03	±0.04	±0.02	±0.07	±0.05	\

and time.

2.6.3. Multiple wavelet coherence

MWC is a special case of wavelet analysis extended from the relationship of binary time series to multivariate time series at different time scales and frequencies (Hu & Si, 2016; Hu et al., 2017; Su et al., 2019). Given a response variable Y and multiple predictor variables X ($X = \{X_1, X_2, \ldots, X_L\}$), the MWC at scale s and location τ, $\rho_m^2(s,\tau)$, can be expressed as:

$$\rho_m^2(s,\tau) = \overleftrightarrow{W}^{Y,X}(s,\tau)\frac{\overleftrightarrow{W}^{X,X}(s,\tau)^{-1}\overleftrightarrow{W}^{Y,X}(s,\tau)^*}{\overleftrightarrow{W}^{Y,Y}(s,\tau)} \quad (9)$$

where $\overleftrightarrow{W}^{X,X}(s,\tau)$ and $\overleftrightarrow{W}^{Y,Y}(s,\tau)$ are the matrix of smoothed auto- and cross-wavelet power spectra among multiple predictor variables X and the matrix of smoothed wavelet power spectrum of the response variable Y, respectively. $\overleftrightarrow{W}^{Y,X}(s,\tau)$ is the matrix of the smoothed cross-wavelet power spectra between the response variable Y and predictor variables X. $\overleftrightarrow{W}^{Y,X}(s,\tau)^*$ denotes the complex conjugate of $\overleftrightarrow{W}^{Y,Y}(s,\tau)$.

For both WTC and MWC, statistical testing was done against red noise as the null hypothesis, which can be modeled by a first-order autoregressive process requiring >1000 random realizations (Grinsted et al., 2004). The Monte Carlo method was adopted in this study to determine the 5 % significance of WTC and MWC, which is commonly applied for hydrological and ecological data sets (Maraun & Kurths, 2004; Carey et al., 2013). Because the time series are not cyclical, edge artifacts exist. The region of the wavelet spectrum in which edge effects become important is defined as the Cone of Influence (COI), which is marked as lighter shade in the wavelet plots in this paper. For each scale, the significance level was assessed using only the values outside the COI. The global coherence coefficient (GCC), which is the time-averaged value of the WTC at a certain scale (Torrence & Compo, 1998; Liu et al., 2017) was analyzed in this study. The average wavelet coherence (AWC) and the percent area of significant coherence (PASC) relative to the whole wavelet scale-location (out of COI, Hu and Si, 2021) was also calculated. Higher overall AWC and PASC suggest greater dominance (Hu et al., 2017; Cheng et al., 2021). Although inclusion of additional ETa measurements from other sites might increase the coherence with the ETa at a given site, an increase in the PASC value by at least 5 % should be observed before it can be concluded that the additional ETa measurements have practical significance (Hu et al., 2017; Cheng et al., 2021). The wavelet analyses were conducted through Matlab program adopted or adapted from Torrence and Compo, Grinsted and Hu and Si from the website 10.6084/m9.figshare.13031123.

3. Results

3.1. Observations of ET-LYS and ET-EC

Yearly cumulative ET-LYS, ET-EC and ET_0 for the years 2015–2020 are presented in Table 2. Here, the yearly sum of ET-LYS is the average over multiple lysimeters at the same site and with the same soil type, because the standard deviation between lysimeters at the same site and same soil was small. Among all sites, the lysimeters at the Selhausen site filled with Rollesbroich soil (SEro) had on average the largest cumulative ET-LYS (701.6 mm/y), while for the Rollesbroich site (RO) and the

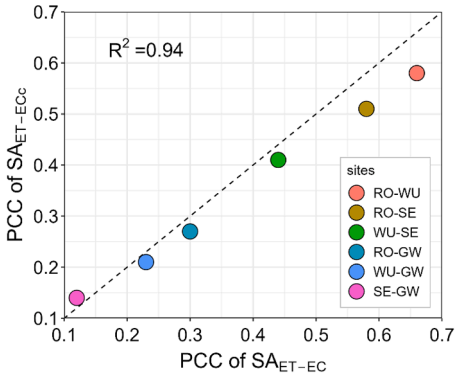

Fig. 4. Scatter plot of Pearson correlation coefficient (PCC) of standardized anomaly (SA) of ET-EC and ET-ECc between the different sites. ET-EC and ET-ECc refer to the ETa measurements from EC without and with energy balance closure, respectively. Dashed line is the 1:1 line.

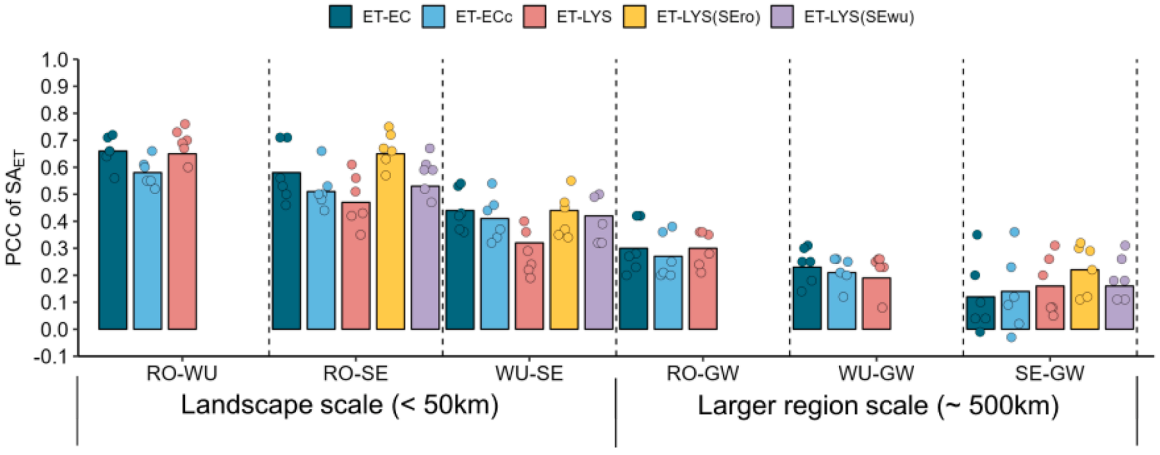

Fig. 3. Pearson correlation coefficient (PCC) for ET-LYS, ET-EC and ET-ECc at the landscape scale. Bars refer to PCC of standardized anomaly of ET-LYS ($SA_{ET\text{-}LYS}$, red bar), standardized anomaly of ET-EC ($SA_{ET\text{-}EC}$, green bar), or standardized anomaly of ET-ECc ($SA_{ET\text{-}ECc}$, blue bar) between different sites for the period 2015–2020. Yellow bar refers to PCC between $SA_{ET\text{-}LYS}$ from lysimeters at SE site filled with soil from RO site (SEro) and another lysimeter site. Purple bar refers to PCC between $SA_{ET\text{-}LYS}$ from lysimeters at SE site filled with soil from WU site (SEwu) and another lysimeter site. Circles denote the PCC for individual years.

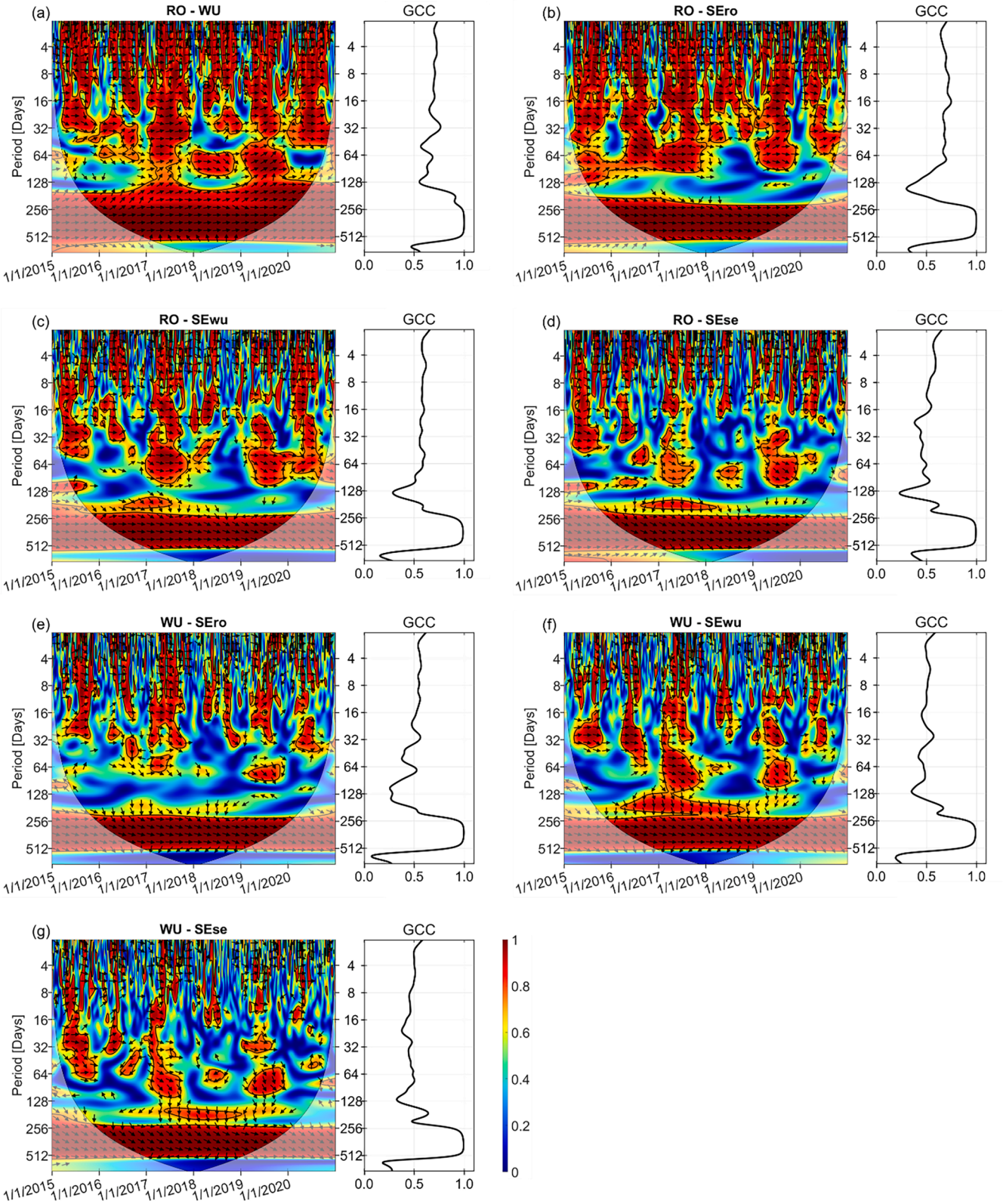

Fig. 5. Wavelet transform coherence (WTC) and global coherence coefficient (GCC) of ET-LYS between (a) RO and WU, (b) RO and SEro, (c) RO and SEwu, (d) RO and SEse, (e) WU and SEro, (f) WU and SEwu, (g) WU and SEse. The vertical axis shows the periodicity up to 770 days. The right part of each panel demonstrates the GCC. The left part of each panel depicts WTC and the horizontal axis shows the study period (from 2015 to 2020 on daily basis). Thick contours indicate significant coherence at 95 % confidence level. The pale region delineates the cone of influence (COI) where edge effect might distort the results. Small arrows show the phase difference between two series (right arrows indicate in-phase (positive) relationship, left arrows indicate out-of-phase (or negative) relationship (180°), and arrows upwards (downwards) indicate the second series leading (lagging) the first by 90°). The color denotes the strength of coherence with the red being high and blue being low.

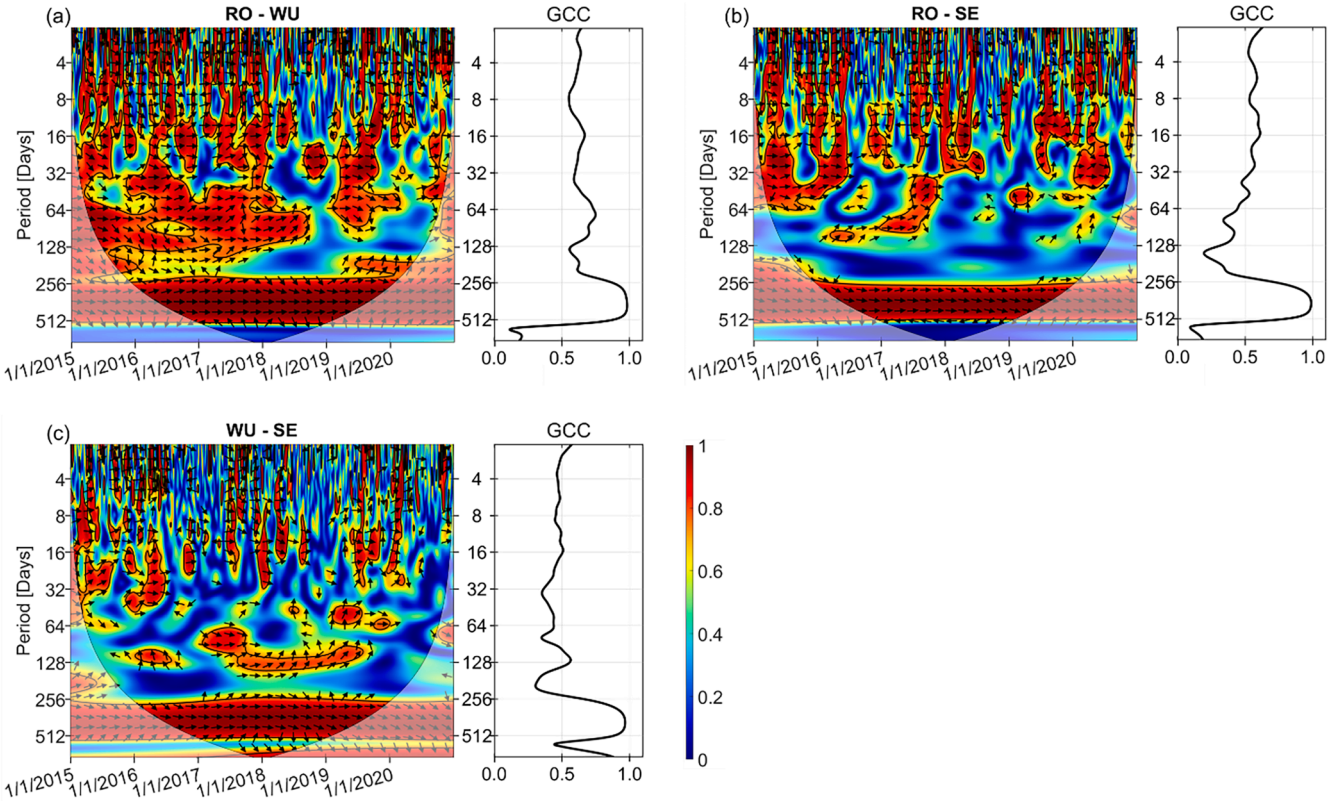

Fig. 6. Wavelet transform coherence (WTC) and global coherence coefficient (GCC) of ET-EC between (a) RO and WU, (b) RO and SE, (c) WU and SE. The vertical axis shows the periodicity up to 770 days. The right part of each panel demonstrates the GCC. The left part of each panel depicts WTC and the horizontal axis shows the study period (from 2015 to 2020 on daily basis). Thick contours indicate significant coherence at 95 % confidence levels against red noise. The pale region delineates the cone of influence (COI) where edge effect might distort the results. Small arrows show phase difference between two series (right arrows indicate in-phase relationship, left arrows indicate out-of-phase relationship (180°), and arrows upwards (downwards) indicate the second series leading (lagging) the first by 90°). The color denotes the strength of coherence.

Graswang site (GW) ET-LYS were slightly smaller (676.8 mm/y and 651.4 mm/y, respectively) and for the Wüstebach site (WU) much smaller (406.1 mm/y). At the Selhausen site (SE), lysimeters with other soil types had a much lower ET-LYS than those of SEro: for lysimeters with Wüstebach soil (SEwu) 556.4 mm/y and for lysimeters with Selhausen soil (SEse) 549.2 mm/y. The measured ET-LYS were close to ET_0 for the wet grassland RO and GW sites. In 2018 however, with a marked hot and dry summer period, both at the RO site and GW site ET-LYS was clearly smaller than ET_0 (up to 10 % and 6 %, respectively). On the other hand, for the drier and warmer SE site ET-LYS was in general smaller than ET_0, but strongly dependent on the soil type. For lysimeters SEse, ET-LYS was on average over the six years 27 % smaller than ET_0. For SEro the difference with ET_0 was much smaller (7 % on average). The largest differences between ET-LYS and ET_0 were found for the year 2018, with ET-LYS being 40 % smaller than ET_0 for SEse. This shows that the ETa in the dry year 2018 at SE was strongly limited by the lack of water, which is in line with previous investigation at SE for grassland (Forstner et al., 2021) and the crop oat (Groh et al., 2022). Finally, for WU ET-LYS was much smaller than ET_0 (37 % on average over the six years) although WU is a wet site. This is because the lysimeter is located in the forest shadow and reduced sunlight reaching the grasses can result in lower rates of ETa compared to ET_0 that was based on above-canopy radiation measurements. Among the six years, year 2020 witnessed the highest ET_0 at all the three sites in western Germany (768.1 mm/y, 706.3 mm/y and 807.3 mm/y at RO, WU, and SE, respectively), whereas the largest ET_0 was 705.8mm/y in 2018 at GW in southern Germany.

At RO and GW, the yearly sum of uncorrected ET-EC was on average 22 % and 28 % smaller than that of ET-LYS, respectively. This is in accordance with the findings reported by Gebler et al. (2015) and Mauder et al. (2018). For SEro, the yearly sum of ET-LYS was markedly larger than that of ET-EC (26.8 %). However, for SEwu and SEse ET-LYS was only slightly larger than ET-EC at the SE site (7.7 % and 6.5 %, respectively). The biomass production on the lysimeters corroborate these findings with more biomass on the SEro lysimeters than the other lysimeters. These differences in ET and biomass production might be related to the soil properties, so that SEro lysimeters are less affected by drought than SEwu and SEse. We found that in July and August, ET-LYS from SEro lysimeters is much higher than that from SEse lysimeters (the difference was 37 mm on average, Figure S1). This disparity can be explained by the fact that the SEse lysimeters were generally bare soil for most of the time during the two months which led to less transpiration by the plants (Table S6), while on the SEro lysimeters grass was growing. In WU, the average annual ET-EC of the six years was 30 % higher than ET-LYS, which agrees well with a previous investigation at the site, where ET-EC was 41 % higher than for the forest meadow (Bogena et al., 2015). This is again due to the fact that, on the one hand, the lysimeter at the WU site is located in the forest shade, and thus has a significant lower energy input than the forest area, and, on the other hand, the ET-EC in Wüstebach measures ETa over the forested footprint of a spruce stand (*Picea abis* L.), which has a much higher leaf area index than the local grassland.

With the correction of the energy balance deficit using the Bowen ratio method, the yearly sum of ET-ECc increased substantially (Table 2). The RO site had the most significant increase where the annual ET-ECc was on average 16.9 % higher than ET-EC. ET-ECc is closer to ET-LYS than ET-EC, with the difference of annual ETa measurements between EC and lysimeter on average reducing from 22 % to 5.6 %. Similarly, ET-ECc at the GW site also showed a clear increase and

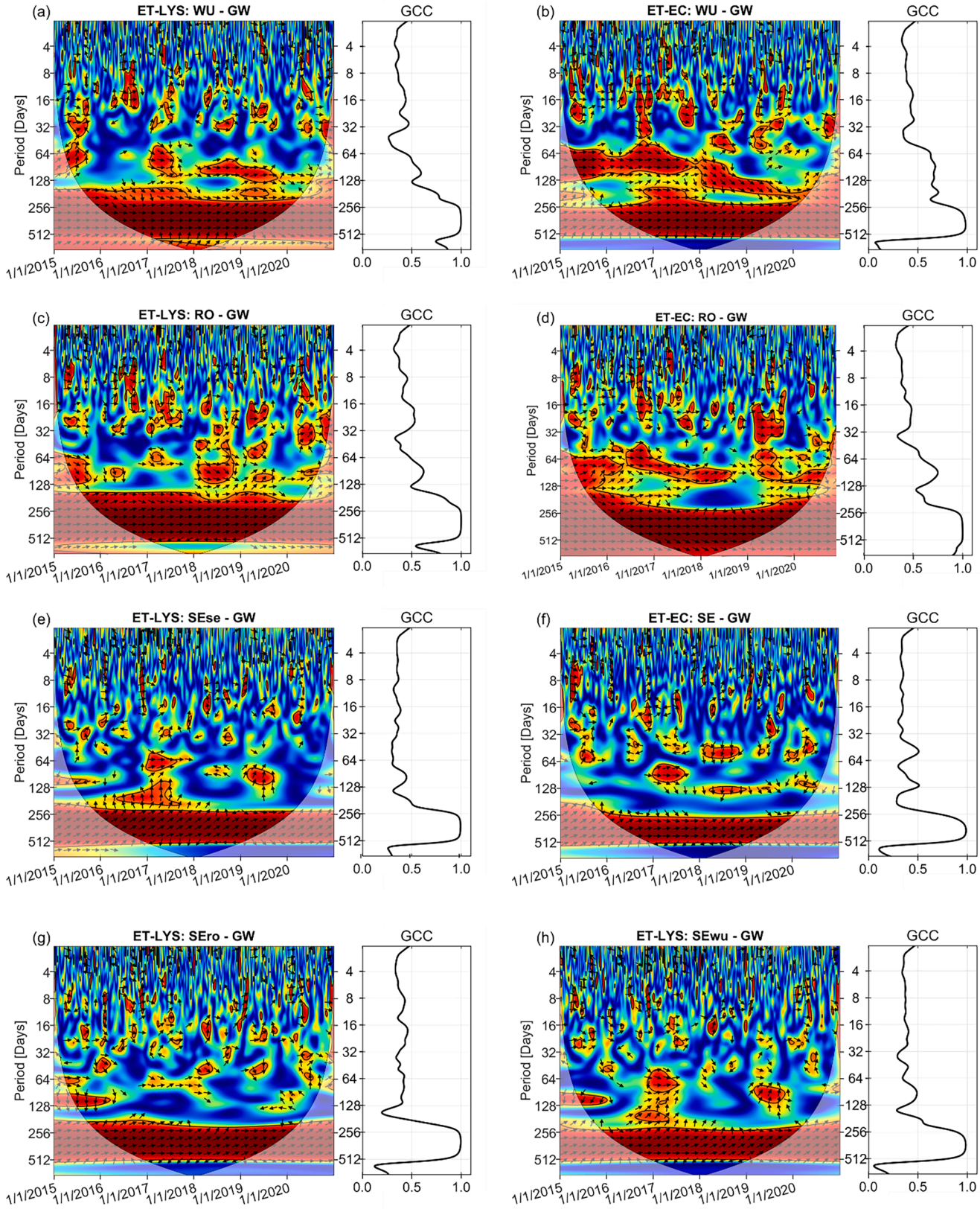

Fig. 7. Wavelet transform coherence (WTC) and global coherence coefficient (GCC) of ET-LYS between (a) WU and GW, (b) RO and GW, (c) SEse and GW, (g) SEwu and GW and (h) SEro and GW, and WTC of ET-EC between (d) WU and GW, (e) RO and GW and (f) SE and GW. The vertical axis shows the periodicity up to 770 days. The right part of each panel demonstrates the GCC. The left part of each panel depicts WTC and the horizontal axis shows the study period (from 2015 to 2020 on daily basis). Thick contours indicate significant coherence at 95 % confidence level. The pale region delineates the cone of influence (COI) where edge effect might distort the results. Small arrows show phase difference between two time series (right arrows indicate in-phase relationship, left arrows indicate out-of-phase relationship (180°), and arrows upwards (downwards) indicate the second series leading (lagging) the first by 90°). The color denotes the strength of coherence.

Table 4
Average wavelet coherence (AWC) and percent area of significant coherence (PASC) values for the wavelet coherence of ET-LYS or ET-EC between two sites at the landscape scale.

ET-LYS			ET-EC		
Site	AWC	PASC (%)	Site	AWC	PASC (%)
RO - WU	0.73	58	RO - WU	0.65	47
RO - SEse	0.56	34	RO - SE	0.53	32
RO - SEro	0.68	51			
RO - SEwu	0.60	39			
WU - SEse	0.53	29	WU - SE	0.52	27
WU - SEro	0.54	30			
WU - SEwu	0.55	32			

Table 5
Average wavelet coherence (AWC) and percent area of significant coherence (PASC) values for the wavelet coherence of ET-LYS or ET-EC between two sites at the larger regional scale.

ET-LYS			ET-EC		
Sites	AWC	PASC	Sites	AWC	PASC
RO - GW	0.56	30	RO - GW	0.58	37
WU - GW	0.54	29	WU - GW	0.52	30
SEse - GW	0.45	20	SE - GW	0.43	18
SEro - GW	0.47	21			
SEwu - GW	0.45	20			

was closer to ET-LYS, but still with a difference of 17 %. At the WU and SE sites, ET-ECc increased by 6.4 % and 17 % compared to ET-EC, respectively.

Fig. 2 shows the average yearly cycle of ET-LYS, ET-EC, ET-ECc and ET_0 at monthly resolution for the study period. All four sites show a distinct yearly cycle. In summer (June to August) the monthly cumulative ET-LYS values for RO, WU, and GW were larger than in other seasons, with peak values in RO in June of 112.0 mm close to ET_0 (109.8 mm), in WU for July of 72.8 mm and in GW for July of 118.1 mm. ET-LYS for RO was obviously higher than ET_0 in May and June, suggesting that in these months grass heights were larger than the reference grass height of 12 cm combined with ETa which was not limited by soil moisture but by energy. The highest monthly ET-LYS in SE was found in May for all soils and land surface cover types, namely 105.1 mm (SEro), 86.0 mm (SEwu), and 97.3 mm (SEse). For SEse, this can be explained by the fact that in May the crops were growing and therefore ETa was high, while in summer ETa decreased due to the end of the growing season. For the grass, this is most likely related to the fact that in summer at the SE site ETa is often reduced due to drought, while RO and WU are less affected by drought stress given the higher precipitation and lower ET_0, compared to SE. However, also the change in the growing season duration combined with less precipitation might affect the ETa difference between sites. Forstner et al. (2021) demonstrated that transferring soil from RO to SE increases the length of the growing season by an average of 36 days. December witnessed the lowest average monthly cumulative ET-LYS at the RO, WU, and SE sites, but the lowest monthly ET-EC and ET-ECc was registered in January.

Over the six years, the percentage of gap-filled ET-LYS at RO, WU and SE was on average 10.2 % and at GW 48.9 % (Table 2). The higher percentage at GW is related to snow cover (with over 80 % and even up to 100 % of missing data in January, February, March and December, Tables S3 and S4) and the frequent chamber measurements performed on the lysimeters which disturbed the lysimeter ET measurements. The percentage of gap-filled ET-EC data was higher than for ET-LYS at all sites, with an average of 36.3 % across the four sites, and for WU it was even up to 65.3 % in 2018 (Table 2). More data gaps occurred during night than that during daytime (Table S5) due to more stable conditions with lower wind speeds and reduced turbulence during night (Straaten & Weber, 2021). Given the fact that ETa is primarily composed of daytime ETa (Ding et al., 2010; Groh et al., 2019; Han et al., 2021), the high gap-filling percentage of nighttime ETa does not necessarily reduce the reliability of the data. In addition, both lysimeters and EC had more missing data in winter (Table S4), which is related to snow and frost (lysimeters, Tables S1-S3) and stable conditions where the EC data is not reliable.

3.2. Pearson correlations for ET-LYS and ET-EC at different spatial scales

3.2.1. Plot and landscape scale

Table 3 shows the average PCCs of $SA_{ET\text{-}LYS}$ between different individual lysimeters at the same measurement site. The lysimeters with the same soil origin at the same site showed high correlations (>0.9) and very low standard deviations (<0.08). The high PCCs indicate that the replications of lysimeter worked well and lysimeter measurements provide representative information at the plot scale.

Given the fact that lysimeter measurements are representative at the plot scale with very high correlations among different lysimeters at the same site, we used the average ET-LYS for different lysimeters with the same soil at the same site to perform the succeeding analyses. Fig. 3 shows PCCs for ET-LYS, ET-EC and ET-ECc between different sites. At the landscape scale (separation distances < 50 km), PCCs of $SA_{ET\text{-}LYS}$ varied between 0.32 and 0.65. The correlation between the WU and RO site was 0.65 and the two sites have a similar climate and are not separated far in space (13 km). Correlations were smaller between WU (or RO) and the SE site, which is related to differences in precipitation and potential evapotranspiration (ET_0), as well as soil type between WU or RO on one hand and SE on the other hand. The lowest correlation of 0.32 was found between WU and the lysimeters SEse. In summary, $SA_{ET\text{-}LYS}$ show moderate correlations between lysimeters which are between 10 and 50 km separated in space.

Next, we compare the PCCs of $SA_{ET\text{-}LYS}$ and $SA_{ET\text{-}EC}$ across different sites over the 6 years period at the landscape scale (Fig. 3). The PCC between RO and WU are very similar for $SA_{ET\text{-}LYS}$ and $SA_{ET\text{-}EC}$ (0.65 and 0.66, respectively) despite the different vegetation at WU for the EC station (forest) and the lysimeters (grass). In addition, as pointed out before, the lysimeters at the WU site are located in a forest meadow which is often shaded (morning and evening hours) by the surrounding spruce stand, whereas the EC station measures ETa above the forest canopy. The PCC was high between RO and the SEro lysimeters (0.65). This could be related to the fact that the same soil and vegetation on the lysimeters at both sites lead to a similar ETa response. On the other hand, the PCC for ET-LYS between the lysimeters at RO and the lysimeters in SE filled with WU soil (SEwu) was slightly lower than the PCC for ET-EC (0.58) between RO and SE. Finally, PCC for ET-LYS between lysimeters in RO and lysimeters in SE filled with SE soil (SEse) was lower than PCC for ET-EC between RO and SE (0.47 versus 0.58), and showed relative high variation between years with values varying between 0.61 (2015) and 0.35 (2018). The differences between the years can be related to the different crop types and crop rotation (with different harvest times) for lysimeters and EC at the SE site (Tables S6 and S7).

Also for WU and SE, despite the distance between the two sites of about 50 km, a moderate PCC for ET-LYS measured by lysimeter SEse was found (0.32), which was slightly smaller than for ET-EC (0.44). The PCCs of $SA_{ET\text{-}LYS}$ between the two sites show a similar pattern as function of the different soil types as RO and SE. Lysimeters SEro showed the strongest correlation (0.44) with lysimeters in WU, closely followed by the lysimeters SEwu (0.42).

After forcing energy balance closure, the PCCs of $SA_{ET\text{-}ECc}$ were all lower than $SA_{ET\text{-}EC}$ at the landscape scale, varying between 0.41 and 0.58. The PCC of $SA_{ET\text{-}ECc}$ even became lower than PCC for $SA_{ET\text{-}LYS}$ between RO and WU sites (Fig. 3). Overall, although the distances across the three sites vary from 10 to 50 km, PCC for ET-LYS was moderately strong, and similar to the PCC for ET-EC and ET-ECc.

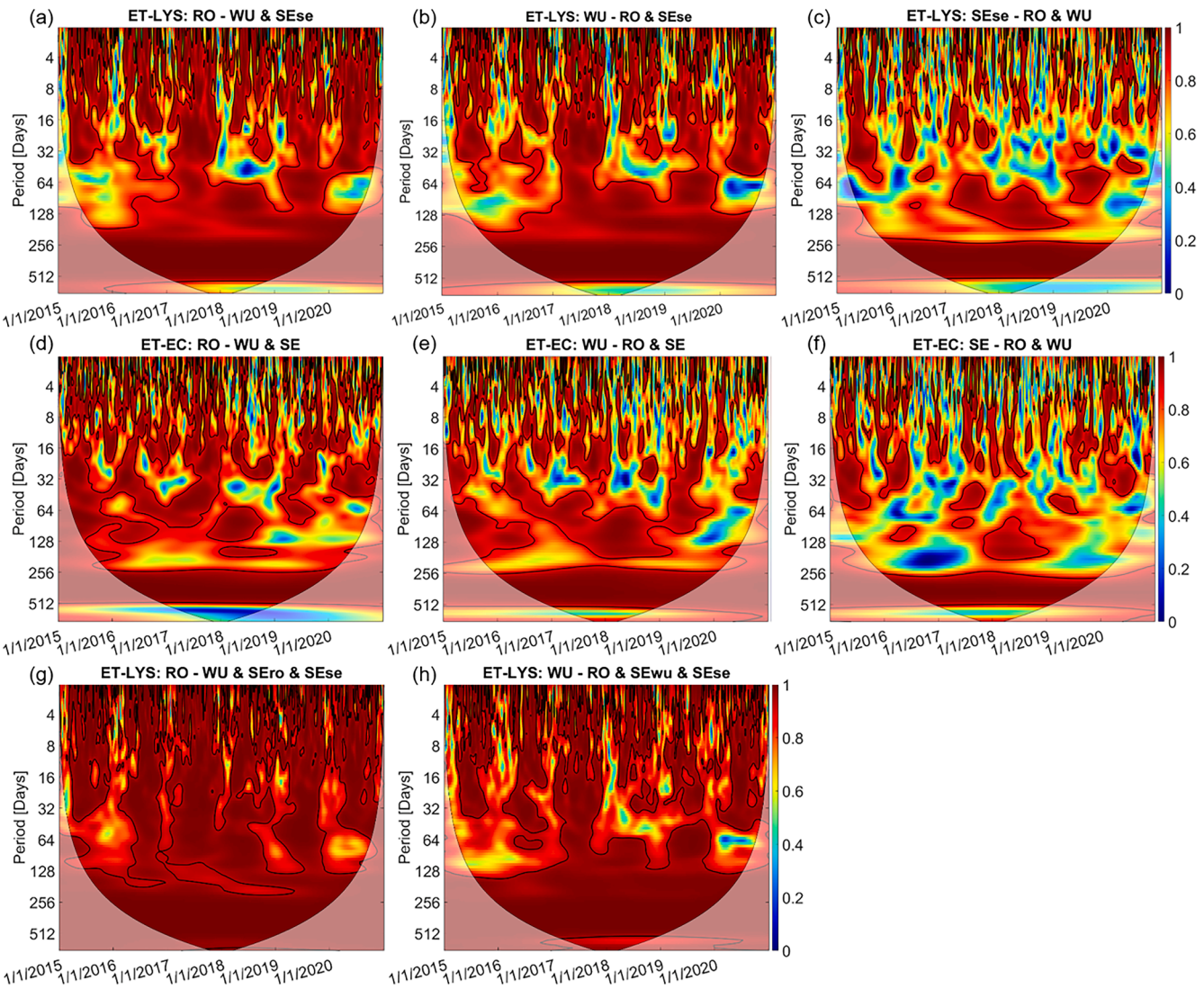

Fig. 8. Two-site scenario of multiple wavelet coherence (MWC) at the landscape scale. The vertical axis shows the periodicity up to 770 days, and the horizontal axis the study period (from 2015 to 2020 on daily basis). Thick contours indicate significant coherence at 95 % confidence level. The pale region delineates the cone of influence (COI) where edge effect might distort the results. The color denotes the strength of coherence.

3.2.2. Larger regional scale (~ 500km)

For the larger regional scale, the PCC was clearly lower than at the landscape scale, varying between 0.16 and 0.3 for $SA_{ET\text{-}LYS}$ and between 0.12 and 0.3 for $SA_{ET\text{-}EC}$ (Figure 3). At this scale, RO and GW had the highest correlations, both for $SA_{ET\text{-}LYS}$ and $SA_{ET\text{-}EC}$ (0.3). The distance between RO and GW is 485km. The strong PCC may be related to the fact that both are extensively managed grassland sites and in general not much affected by drought, as both sites are rather energy than water limited ecosystems. Between WU and GW, PCC was lower and for $SA_{ET\text{-}LYS}$ slightly lower than for $SA_{ET\text{-}EC}$, with values of 0.19 and 0.23, respectively. Between SE and GW, $SA_{ET\text{-}LYS}$ shows higher PCC than $SA_{ET\text{-}EC}$ (0.12) irrespective of soil and vegetation type, namely 0.16 (SEse), 0.22 (SEro) and 0.16 (SEwu). PCCs of $SA_{ET\text{-}EC}$ and $SA_{ET\text{-}LYS}$ between GW and the arable land SE (or lysimeter SEse) varied a lot between years.

The relationship between the PCC for ET-ECc and PCC for ET-EC was close to the 1:1 line with R^2 of 0.94, although there was a systematically slightly lower correlation for ET-ECc than for ET-EC (Fig. 4). Interestingly, with the increase of the distance between sites, the difference between PCCs for ET-EC and PCCs for ET-ECc decreased (regardless of landscape scale or larger regional scale), with the difference reduced from 0.08 to −0.02. Though yielding different PCC values, correction of energy balance for ET-EC did not change the results of the comparison with ET-LYS at larger regional scale (Fig. 3), indicating that the results are robust. Overall, the correlation for ET-LYS was not much smaller than that for ET-EC, suggesting that the lysimeter can provide as much information as an eddy covariance measurement. In addition, although the sites are far separated in space, still a small correlation in ET was found, indicating that weather systems play a role in driving ETa. However, given the low correlations at this separation distance of 500 km, the information content of lysimeters is quite limited for the larger regional scale.

3.3. Wavelet coherence of ET-LYS and ET-EC

Given the similar PCC results for corrected ET-ECc, we continue the analysis with uncorrected ET-EC. To explore the correlations for ET-LYS and ET-EC at various temporal scales, the wavelet transform coherence (WTC) was computed. Figure S2 presents the continuous wavelet transform (CWT) ET-LYS and ET-EC for each site. Figs. 5, 6 and 7 show the WTC results for ET-LYS and ET-EC between any two sites for the 6-year time series and at which temporal frequencies coherence of the ETa time series appears between two sites.

When analyzing the CWT, both ET-LYS and ET-EC at each site showed significant annual cycle, and a cycle between 1 and 16 days

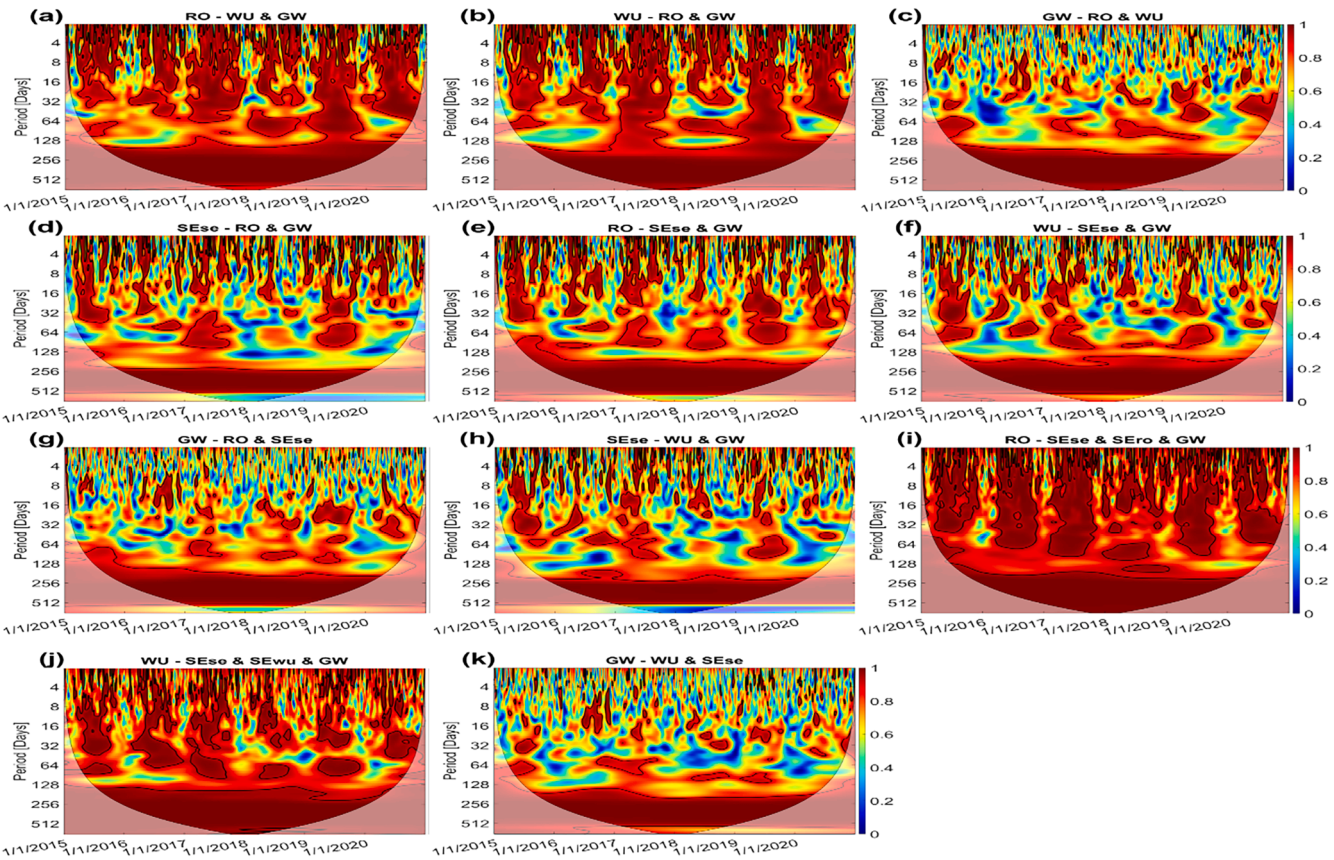

Fig. 9. Two-site scenario of multiple wavelet coherence (MWC) of ET-LYS at the larger regional scale. The vertical axis shows the periodicity up to 770 days, and the horizontal axis the study period (from 2015 to 2020 on daily basis). Thick contours indicate significant coherence at 95 % confidence level. The pale region delineates the cone of influence (COI) where edge effect might distort the results. The color denotes the strength of coherence.

appeared in the middle of each year (Figure S2).

In the cross-wavelet analysis, at landscape spatial scale, from Figs. 5 and 6 it can be seen that the WTC between any two measurement sites was markedly significant both for ET-LYS and ET-EC at the semi-annual and annual scale (180 −512 days), where the GCC stayed at a consistently high value, even up to 1. This is intuitive since ET-LYS and ET-EC at each site all showed a marked annual cycle (Fig. S2). The significant WTC suggest that the semi-annual (winter to summer) trend and the between-year trend on ETa are very similar. This is logical as the winter and summer variations on ETa exhibit the most substantial changes, and the between-year variations can also be significant. Both lysimeter and EC can capture these distinctive features. Among these, RO exhibits perfectly in-phase (positive) correlations with WU irrespective of ET-LYS or ET-EC, whereas RO and WU lag SE by <1 month for all lysimeter soils and ET-EC, as indicated by the arrows in the figures.

For the RO-WU couple, the coherence at a scale of around 1 day and 1 month was intermittent and generally in phase both for ET-LYS and ET-EC, with less coherence during winter (Figs. 5a and 6a). But ET-EC displays more disruptions than ET-LYS at this time scale, especially in the drier years (2018–2020), when ET-EC lost coherence during summer months. Overall, the AWC and PASC for ET-LYS were similar to those for ET-EC (0.73 and 58 % for ET-LYS and 0.65 and 47 % for ET-EC, respectively, Table 4).

ET-LYS from RO and WU show similar wavelet coherence spectra with the SE lysimeters, yet RO shows greater coherence than WU. For the RO-SEse and the WU-SEse couple, the WTC results show intermittent coherence for the 1- to 16-day period and scattered coherence for the 16-day to half-year scale (Figs. 5 and 6). Most coherence is positive with varying phase shift, but at a scale of around 90 days, the coherence turns negative between May and August 2018, with arrows pointing to the left. Compared with ET-LYS, ET-EC between RO and SE has smaller AWC (0.53) and PASC (32 %). For the WU-SE couple, ET-EC shows more frequent breaks at a scale <16 days compared to ET-LYS.

The RO-SEro, RO-SEwu, WU-SEro and WU-SEwu couples all show fragmentary coherence at small scales of 1 day to 1 month (Figs. 5 and 6). GCC is at a lower level for WU couples than RO couples. At this scale, very weak or even no coherence was found in winter due to the lower signal to noise ratio in winter, given small ET and the role of measurement errors. Coherence was also weak in spring and autumn, which may be related to the difference in beginning and end of growing season within the Eifel and at Selhausen (Forstner et al., 2021). Again, the coherence in 2018 was significantly smaller compared to other years revealed by more blue area.

Compared to the landscape scale, both ET-LYS and ET-EC at the larger regional scale show less area with significant coherence (compared to Fig. 7) and smaller AWC and PASC (Table 5), but there is still significant coherence at some temporal scales. Significant annual coherence prevails during the entire study period for all pairs of sites for both ET-EC and ET-LYS. RO and WU have in-phase (positive) coherence with GW, whereas the wet GW site lags the dry SE site, irrespective of the soil and vegetation type at SE, with arrows pointing slightly upwards.

ET-EC between RO and GW have the highest AWC (0.58) and PASC (37 %) at the larger regional scale, followed by ET-EC between WU and GW (0.52 for AWC and 30 % for PASC). The ET-LYS data show slightly less coherence than ET-EC with 30 % PASC for the RO-GW couple and 29 % for the WU-GW couple. ET-EC between RO (or WU) and GW displays sometimes significant coherence at a time scale around 64–128 days, more than for ET-LYS. For the WU-GW couple, ET-EC shows significant coherence at the scale around 90 days during the entire time periods, while the arrows point to the right before 2017 and pointing right down

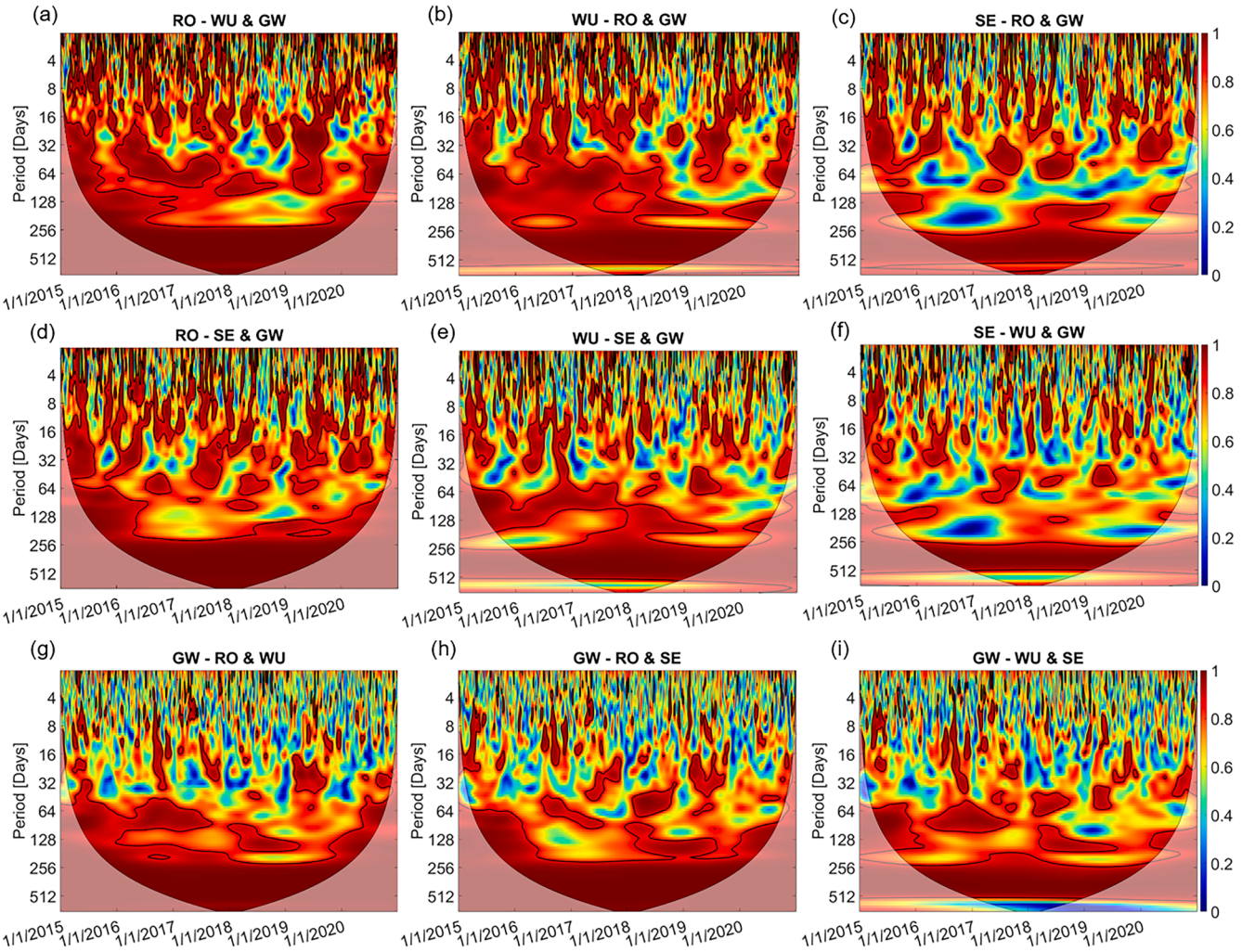

Fig. 10. Two-site scenario of multiple wavelet coherence (MWC) of ET-EC at the larger regional scale. The vertical axis shows the periodicity up to 770 days, and the horizontal axis the study period (from 2015 to 2020 on daily basis). Thick contours indicate significant coherence at 95 % confidence level. The pale region delineates the cone of influence (COI) where edge effect might distort the results. The color denotes the strength of coherence.

from 2018 onwards indicating that GW lags WU. On the other hand, significant coherence at the time scale around 90 days for ET-LYS between March 2018 and November 2019 shows no lag.

For the SE and GW sites, ET-LYS has higher AWC and PASC than ET-EC (Table 5), but both ET-LYS and ET-EC show a low significant coherence at the scales other than the annual scale.

3.4. Combined ETa measurements from multiple sites

In this section, we present the results of the analysis using multiple wavelet coherence across various sites. Overall, we observe significant continuous annual periodic characteristics prevailing both for ET-LYS and ET-EC at the landscape scale and larger regional scale (Figs. 8–11).

At the landscape scale, compared with WTC results (on average 0.6 for ET-LYS and 0.57 for ET-EC, Tables 4 and 5), the two-site scenario significantly improves AWC (on average 0.86 for ET-LYS and 0.79 for ET-EC, Table 6). Fig. 8 shows that the consistency and coherence for the scales of 1 day to 3 months is also notably improved compared with Figs. 5 and 6. The best combination is WU and SE sites, which account for 50 % to 71 % of the ETa variation at the RO site. Conversely, the least effective combination is RO and WU sites which account only for 30 % of the ETa variation at the SE site. Interestingly, when adding one lysimeter measurement which contains the same soil and vegetation from the response site, MWC increases significantly (from 0.86 to 0.94 for the RO site and from 0.85 to 0.91 for the WU site). However, PASC does not show a significant increase (8 % increase for RO and 1 % decrease for WU). This could be related to the overlapping effects due to the collinearity among the lysimeter measurements at the SE site.

At the larger regional scale, two-site combination shows higher AWC than WTC, with AWC>0.7 (Table 7). The highest AWC is achieved by the combination of ET-LYS from SEse, SEro and GW to predict RO (0.91). Meanwhile, the AWC for ET-LYS are not lower than for ET-EC. When adding another site, PASC for ET-LYS and ET-EC all increase, ranging from 0.84 to 0.97. However, when adding a SE site, the PASC does not improve.

Shifting from the two-site to the three-site scenario, we note a pronounced improvement in AWC both for ET-LYS and ET-EC (on average 0.91 and 0.88, respectively) and in PASC for ET-LYS (on average 52 %). However, the increase of PASC for ET-EC (by 4 % on average) is small. Likewise, when adding SEro or SEwu, the AWC is the highest.

4. Discussion

4.1. Overall assessment of correlations

The spatial correlations of ETa as observed are affected by the hydrological status of the system, i.e. whether ET is energy limited or water limited. This status can be characterized according to the Budyko

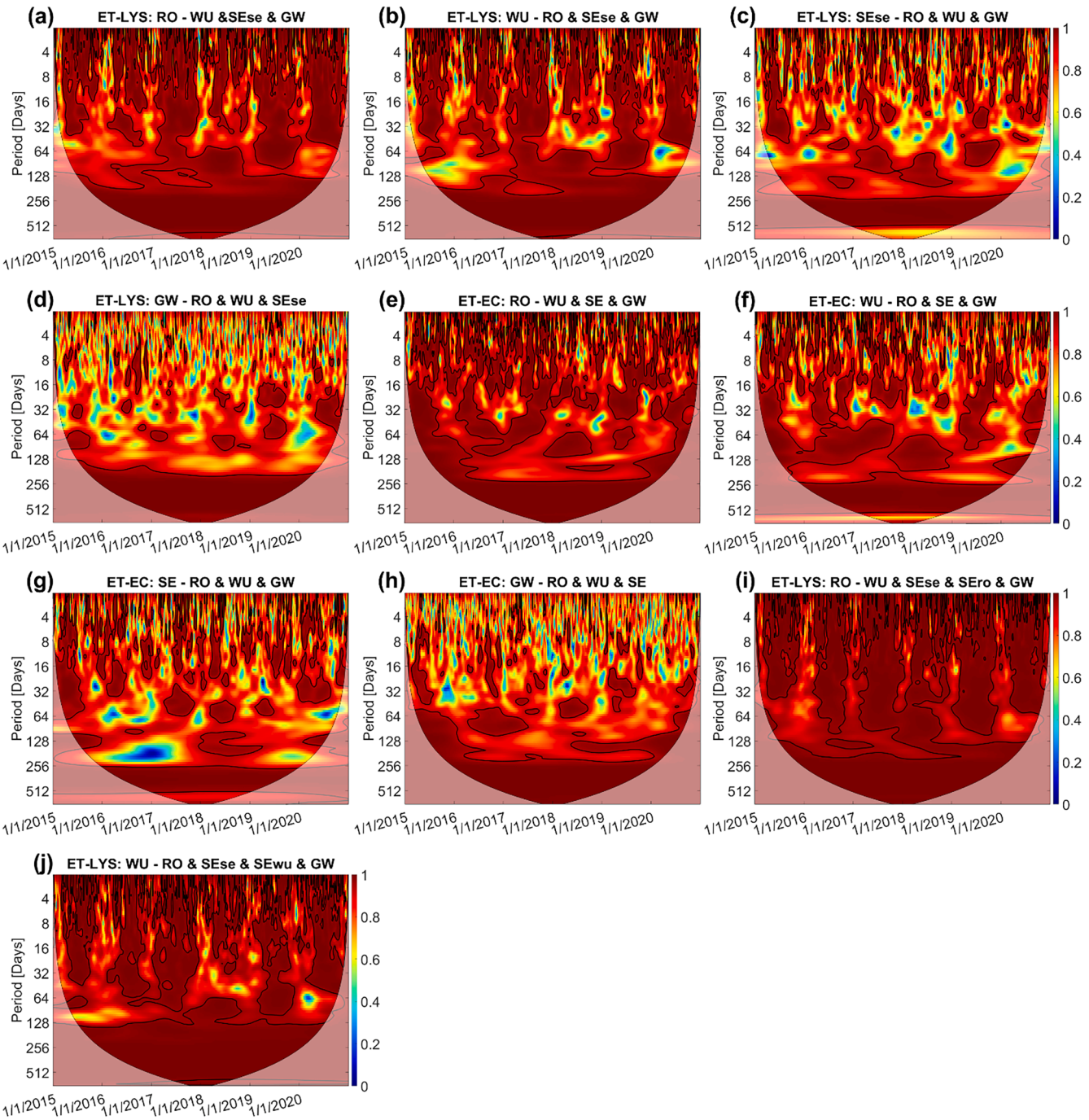

Fig. 11. Three-site scenario of multiple wavelet coherence (MWC) at the larger regional scale. The vertical axis shows the periodicity up to 770 days, and the horizontal axis the study period (from 2015 to 2020 on daily basis). Thick contours indicate significant coherence at 95 % confidence level. The pale region delineates the cone of influence (COI) where edge effect might distort the results. The color denotes the strength of coherence.

framework, which is a widely used conceptual model by linking ETa with ET_0 and precipitation (Akbar et al., 2018; Rahmati et al., 2020). The ETa correlations between two sites with the same hydrological status are higher than between those with different hydrological status irrespective of ET-LYS or ET-EC. For example, the RO-WU couple has the highest PCC among the lysimeter pairs at the landscape scale and the PCCs for the RO-GW couple and the WU-GW couple are higher than for the SE-GW couple at the large regional scale (Fig. 3). This is because RO, WU and GW are mostly energy-limited sites that are not easily affected by drought, whereas SE is a site which has sometimes water-limited conditions (Figure S3). It would be interesting to extend the investigation further including more water limited sites to calculate also correlations between water limited sites. However, unfortunately high resolution high quality lysimeter data are scarce, especially for semi-arid and arid sites.

The vegetation and soil also affect the correlations between sites. Lysimeters for different sites have a higher correlation, and higher PASC with coherence at more temporal scales, if they contain the same soil, and the correlation is weaker if the soil in the two lysimeters has a different texture. This could be observed with the translocated lysimeters from energy-limited sites to water-limited sites (Rahmati et al., 2020), comparing for example RO-SEro vs. RO-SEse as well as WU-SEwu vs. WU-SEse (Fig. 5 and Table 4).When adding an additional ETa timeseries from the lysimeter filled with the same soil and vegetation as

Table 6
Main statistics of multiple wavelet coherence (MWC) of ET-LYS (or ET-EC) between sites at the landscape scale. AWC refers to average multiple-wavelet coherence. PASC refers to the percent area of significant coherence. The symbol "&" means combination, e.g., RO - WU & SEse means the coherence between ET-LYS at the RO site and the combination of ET-LYS from lysimeters at the WU site and SE site filled with local soil.

ET-LYS			ET-EC		
Two sites	AWC	PASC	Two sites	AWC	PASC
RO - WU & SEse	0.86	64	RO - WU & SE	0.82	50
RO - WU & SEse & SEro	0.94	71			
WU - RO & SEse	0.85	59	WU - RO & SE	0.81	46
WU - RO & SEse & SEwu	0.91	58			
SEse - RO & WU	0.75	35	SE - RO & WU	0.74	33

Table 7
Main statistics of multiple wavelet coherence (MWC) of ET-LYS (or ET-EC) between sites at the larger regional scale. AWC refers to average multiple-wavelet coherence. PASC refers to the percent area of significant coherence. The symbol "&" means combination, e.g., RO - WU & GW means the coherence between ET-LYS at the RO site and the combination of ET-LYS measured by lysimeters at the WU site and lysimeters at the GW site.

ET-LYS			ET-EC		
Two sites	MWC	PASC	Two sites	MWC	PASC
RO - WU & GW	0.86	59	RO - WU & GW	0.82	52
RO - SEse & GW	0.79	41	RO - SE & GW	0.82	51
RO - SEse & SEro & GW	0.91	56			
WU - RO & GW	0.84	59	WU - RO & GW	0.82	50
WU - SEse & GW	0.75	37	WU - SE & GW	0.76	37
WU - SEse & SEwu & GW	0.86	43			
SEse - RO & GW	0.72	31	SE - RO & GW	0.75	37
SEse - WU & GW	0.70	28	SE - WU & GW	0.70	24
GW - RO & WU	0.73	34	GW - RO & WU	0.75	40
GW - RO & SEse	0.72	29	GW - RO & SE	0.75	38
GW- WU &SEse	0.70	28	GW- WU &SE	0.71	29

Table 8
Main statistics of multiple wavelet coherence (MWC) of ET-LYS (or ET-EC) between sites at the larger regional scale. AWC refers to average multiple-wavelet coherence. PASC refers to the percent area of significant coherence. The symbol "&" means combination, e.g., RO - WU & SEse & GW means the coherence between ET-LYS at the RO site and the combination of ET-LYS measured by lysimeters at the WU site, lysimeters at the SE site filled with local soil and lysimeters at the GW site.

ET-LYS			ET-EC		
Three sites	AWC	PASC	Three sites	AWC	PASC
RO - WU & SEse & GW	0.93	62	RO - WU & SE & GW	0.92	57
RO - WU & SEse & SEro & GW	0.97	68			
WU - RO & SEse & GW	0.91	58	WU - RO & SE & GW	0.89	46
WU - RO & SEse & SEwu & GW	0.95	58			
SEse - RO & WU & GW	0.85	32	SE - RO & WU & GW	0.86	34
GW - RO & WU & Sese	0.84	33	GW - RO & WU & SE	0.86	39

the response site, AWC increased significantly (Tables 7 and 8).The correlations among sites for ET-LYS are not much smaller than for ET-EC, although lysimeters have a small surface area (in this study about 1 m^2) compared to the EC footprint. This can be explained by the fact that correlations for ET-EC might be unusually small or correlations for ET-LYS might be higher. The size and shape of the EC footprint vary strongly depending on wind speed and wind direction (Chu et al., 2021). If the EC field is not homogeneous, the ETa is the spatially average over the footprint, and in combination with varying wind speed and direction this footprint might change and thus sample different areas. This footprint heterogeneity might result in lower correlations between EC sites. On the other hand, although a lysimeter has a limited surface area, it can be regarded as a large area with a homogeneous land surface, not affected by random errors due to atmospheric instabilities caused by wind gusts (Widmoser & Michel, 2021), resulting in ETa behaving in a similar way under similar meteorological conditions and similar vegetation. In our study, the EC towers typically only sample one land use. The RO site is almost exclusively constrained to the grassland (Gebler et al., 2015). The EC tower at the WU site is centered in the forest and the footprint reaches approximately 500 m downwind (Rabbel, 2018). For the SE site, 80 % of footprint climatology is within the agricultural field (Paulus et al., 2024). The flux footprint of the GW site was primarily dominated by short grass within a radius of approximately 200 m around the EC tower (Hirschi et al., 2017). For example, the RO and GW sites are the two sites most comparable in our study. The lysimeters have the same soil, vegetation and management as the EC field (Gebler et al., 2015; Widmoser & Michel, 2021). As a result, the correlation of $SA_{ET\text{-}LYS}$ between RO and GW is equal to the correlation of $SA_{ET\text{-}EC}$.. Very weak correlations were found in winter and higher correlation in summer. This may be related to differences in the signal to noise ratio for ETa for the different seasons, which can also be inferred from the randomly changed phase angles in winter, relatively to summer (Fig. 5). Variability was also found across years, with less coherence in 2018, which is marked as drought year (Graf et al., 2020).

4.2. Implications for lysimeter networks

Given the similar spatial correlations for ET-LYS and ET-EC, we argue that the information content of lysimeter ETa measurements is not limited by their small area. Thus, lysimeters can potentially be used to upscale measured ETa after proper consideration of hydrological regime, land cover and other factors. This has also implications for the design of lysimeter networks. Lysimeters can estimate ETa more precisely than EC (smaller systematic and random measurement errors, especially at nighttime the EC method is more affected by measurement problems), with a similar spatial representativity and the ability to also provide precise measurements for the other water balance components (rainfall, non-rainfall, percolation, capillary rise), but at a higher (maintenance) cost. Therefore, there is a need for a larger lysimeter network, in part collocated with the EC network, especially also in semi-arid and arid climates.

Wavelet coherence analysis is a localized spectral analysis, and thus inherent all features of spectral coherence analysis, such as revealing valuable information about the lag in ETa signals between the sites. Additionally, wavelet analysis provides the global wavelet coherence, which is identical to spectral coherence if the two time series are stationary. These localized wavelet coherence and global wavelet coherence are particularly useful when estimating ETa at one site based on data from neighboring sites. Accurate prediction of ETa requires not just an understanding of the correlation between sites, but also about the lag time between their responses. To improve these predictions, further analysis of the correlations of ETa with other drivers, such as weather conditions and soil moisture, across sites is necessary. For example, if we want to estimate ETa at one site but only have data from another site, understanding both the correlation and the lag time of key drivers between the two sites allows us to predict ETa. This could significantly reduce the need for ETa measurement equipment, enabling ETa estimation at a broader scale even with a limited lysimeter or EC network.

Furthermore, examining coherence on a seasonal scale provides insight into the reliability of using lysimeter data to represent ETa at larger spatial scales. For instance, if strong coherence is observed in the summer, we can confidently use lysimeter data to estimate ETa over a wider area during that season. However, during winter, when coherence

might be lower, more caution is needed in extending site-specific ETa data to larger scales. This seasonal variability highlights the importance of understanding temporal coherence patterns to improve both local and regional ETa predictions.

Due to the scarcity of parallel measurements by lysimeters and EC towers, our study sites are not abundant, particularly the lack of water-limited sites, and the land cover of EC sites and the vegetation on lysimeters are not fully compatible in this study. In addition, the study period is still not long enough, thus we do not get full insight into the correlations under different meteorological conditions. Except for these limitations, our work provides important insights to explore the potential of the in-situ ETa lysimeter measurements.

5. Conclusions

This study investigates the information content of actual evapotranspiration (ETa) measurements by lysimeters analyzing correlations of standardized anomalies of measured ETa between four different measurement sites: Wüstebach, Rollesbroich, Selhausen and Graswang, all located in Germany. Wüstebach, Rollesbroich and Selhausen are located in North-Rhine-Westphalia, Germany with separation distances between 0 and 50 km, whereas Graswang is further separated from all other sites (500 km). For the same sites also the correlations of standardized anomalies of ETa measured by the eddy covariance method are calculated. Standardized anomalies of ETa measured by lysimeters showed at the plot scale (~10 m) very high correlations (>0.91), and at the landscape scale (distances ~50 km) moderate correlations (0.3~0.7). Those correlations are not much smaller than for EC and suggest that the small lysimeter footprint gives information on ETa comparable to EC measurements, which have a much larger footprint. In order to analyze correlations also at different spatiotemporal scales a wavelet transform coherence WTC analysis for lysimeters and EC was performed. The strongest coherence is in general found for the yearly cycle and temporal scales <3 months. Correlations are higher in the summer half year than in winter, with variations between years and lower correlations under drought conditions (2018). High multiple wavelet coherence revealed that ETa can be predicted for a certain point with high accuracy with help of values from multiple lysimeters located in the neighborhood of the point (separation distances 10 - 50 km). This study did not analyze in depth the drivers of the representativeness of lysimeter measurements, and how for example drought conditions could reduce the representativeness related to increased spatial heterogeneity of ETa under such conditions. This will be subject of future work.

Funding

This research was funded by China Scholarship Council (CSC), grant number. 202006710010.

CRediT authorship contribution statement

Xiao Lu: Writing – review & editing, Writing – original draft, Visualization, Methodology, Funding acquisition, Formal analysis, Data curation. **Jannis Groh:** Writing – review & editing, Methodology, Formal analysis, Data curation. **Alexander Graf:** Writing – review & editing, Methodology, Formal analysis, Data curation. **Thomas Pütz:** Writing – review & editing, Formal analysis. **Katrin Schneider:** Data curation. **Bingcheng Si:** Writing – review & editing, Methodology. **Harry Vereecken:** Writing – review & editing, Formal analysis, Conceptualization. **Harrie-Jan Hendricks Franssen:** Writing – review & editing, Supervision, Methodology, Formal analysis, Conceptualization.

Declaration of competing interest

The authors declare that they have no known competing financial interests or personal relationships that could have appeared to influence the work reported in this paper.

Acknowledgments

We acknowledge the support of TERENO and SOILCan, which were funded by the Helmholtz Association (HGF) and the Federal Ministry of Education and Research (BMBF). HJHF and HV also gratefully acknowledge support from the EU eLTER Plus project. Jannis Groh is funded by the Deutsche Forschungsgemeinschaft (DFG, German Research Foundation) (project no 460817082). We are thankful for all the data provided by FLUXNET, eLTER and ICOS and we thank the colleagues at the corresponding lysimeter and eddy covariance station for their kind support: Rainer Gasche and Ingo Völksch (Graswang) and Werner Küpper, Ferdinand Engels, Philipp Meulendick, Rainer Harms, Leander Fürst, Daniel Dolfus, Nils Becker, Martina Kettler and Marius Schmidt (Rollesbroich, Selhausen, and Wüstebach).

Supplementary materials

Supplementary material associated with this article can be found, in the online version, at doi:10.1016/j.agrformet.2024.110288.

Data availability

Data will be made available on request.

References

Akbar R., Gianotti D.J.S., McColl K.A., Haghighi E., Salvucci G.D., & Entekhabi D. (2018). Estimation of landscape soil water losses from satellite observations of soil moisture. J. Hydrometeorol., 19(5), 871–889.

Allen, R.G., Pereira, L.S., Howell, T.A., Jensen, M.E., 2011. Evapotranspiration information reporting: I. Factors governing measurement accuracy. Agric. Water Manag. 98 (6), 899–920. https://doi.org/10.1016/j.agwat.2010.12.015.

Allen, R.G., Pruitt, W.O., Wright, J.L., Howell, T.A., Ventura, F., Snyder, R., Itenfisu, D., Steduto, P., Berengena, J., Yrisarry, J.B., Smith, M., Pereira, L.S., Raes, D., Perrier, A., Alves, I., Walter, I., Elliott, R., 2006. A recommendation on standardized surface resistance for hourly calculation of reference ETo by the FAO56 Penman-Monteith method. Agric. Water Manag. 81 (1–2), 1–22. https://doi.org/10.1016/j.agwat.2005.03.007.

Awada, H., Ciraolo, G., Maltese, A., Provenzano, G., Moreno Hidalgo, M.A., Còrcoles, J.I., 2019. Assessing the performance of a large-scale irrigation system by estimations of actual evapotranspiration obtained by Landsat satellite images resampled with cubic convolution. Int. J. Appl. Earth Obs. Geoinf. 75 (October 2018), 96–105. https://doi.org/10.1016/j.jag.2018.10.016.

Bogena, H.R., Bol, R., Borchard, N., Brüggemann, N., Diekkrüger, B., Drüe, C., Groh, J., Gottselig, N., Huisman, J.A., Lücke, A., Missong, A., Neuwirth, B., Pütz, T., Schmidt, M., Stockinger, M., Tappe, W., Weihermüller, L., Wiekenkamp, I., Vereecken, H., 2015. A terrestrial observatory approach to the integrated investigation of the effects of deforestation on water, energy, and matter fluxes. Sci. China Earth. Sci. 58 (1), 61–75. https://doi.org/10.1007/s11430-014-4911-7.

Bogena, H.R., Montzka, C., Huisman, J.A., Graf, A., Schmidt, M., Stockinger, M., von Hebel, C., Hendricks-Franssen, H.J., van der Kruk, J., Tappe, W., Lücke, A., Baatz, R., Bol, R., Groh, J., Pütz, T., Jakobi, J., Kunkel, R., Sorg, J., Vereecken, H., 2018. The TERENO-Rur hydrological observatory: a multiscale multi-compartment research platform for the advancement of hydrological science. Vadose Zone J. 17 (1), 180055. https://doi.org/10.2136/vzj2018.03.0055.

Bravo, S., González-chang, M., Dec, D., Valle, S., Wendroth, O., 2020. Using wavelet analyses to identify temporal coherence in soil physical properties in a volcanic ash-derived soil. Agric. For. Meteorol. 285–286 (January), 107909. https://doi.org/10.1016/j.agrformet.2020.107909.

Carey, S.K., Tetzlaff, D., Buttle, J., Laudon, H., McDonnell, J., McGuire, K., Seibert, J., Soulsby, C., Shanley, J., 2013. Use of color maps and wavelet coherence to discern seasonal and interannual climate influences on streamflow variability in northern catchments. Water Resour. Res. 49 (10), 6194–6207. https://doi.org/10.1002/wrcr.20469.

Charlier, J.B., Ladouche, B., Maréchal, J.C., 2015. Identifying the impact of climate and anthropic pressures on karst aquifers using wavelet analysis. J. Hydrol. 523, 610–623. https://doi.org/10.1016/j.jhydrol.2015.02.003.

Cheng, Q., Zhong, F., Wang, P., 2021. Baseflow dynamics and multivariate analysis using bivariate and multiple wavelet coherence in an alpine endorheic river basin (Northwest China). Sci. Total Environ. 772, 145013. https://doi.org/10.1016/j.scitotenv.2021.145013.

Chu, H., Luo, X., Ouyang, Z., Chan, W.S., Dengel, S., Biraud, S.C., Torn, M.S., Metzger, S., Kumar, J., Arain, M.A., Arkebauer, T.J., Baldocchi, D., Bernacchi, C., Billesbach, D., Black, T.A., Blanken, P.D., Bohrer, G., Bracho, R., Brown, S., Zona, D., 2021.

Representativeness of eddy-covariance flux footprints for areas surrounding ameriflux sites. Agric. For. Meteorol. 301–302, 108350. https://doi.org/10.1016/J.AGRFORMET.2021.108350.
Cohen, J., 1988. Statistical Power Analysis For the Behavioral Sciences, 2nd Ed. Erlbaum, Hillsdale, NJ.
Cuxart, J., Boone, A.A., 2020. Evapotranspiration over land from a boundary-layer meteorology perspective. Boundary Layer Meteorol. 177 (2–3), 427–459. https://doi.org/10.1007/s10546-020-00550-9.
Denager, T., Looms, M.C., Sonnenborg, T.O., Jensen, K.H., 2020. Comparison of evapotranspiration estimates using the water balance and the eddy covariance methods. Vadose Zone J. 19 (1), 1–21. https://doi.org/10.1002/vzj2.20032.
Denager T., Sonnenborg T.O., Looms M.C., & Bogena H. (2022). Multi-objective Calibration of the Community Land Model Version 5 . 0 Using In-Situ Observations of Water and Energy Fluxes and Variables. July.
Dhungel, R., Aiken, R., Evett, S.R., Colaizzi, P.D., Marek, G., Moorhead, J.E., Baumhardt, R.L., Brauer, D., Kutikoff, S., Lin, X., 2021. Energy imbalance and evapotranspiration hysteresis under an advective environment: evidence from lysimeter, eddy covariance, and energy balance modeling. Geophys. Res. Lett. 48 (1), 1–12. https://doi.org/10.1029/2020GL091203.
Ding, R., Kang, S., Li, F., Zhang, Y., Tong, L., Sun, Q., 2010. Evaluating eddy covariance method by large-scale weighing lysimeter in a maize field of northwest China. Agric. Water Manag. 98 (1), 87–95. https://doi.org/10.1016/j.agwat.2010.08.001.
Evett, S.R., Schwartz, R.C., Howell, T.A., Louis Baumhardt, R., Copeland, K.S., 2012. Can weighing lysimeter ET represent surrounding field ET well enough to test flux station measurements of daily and sub-daily ET? Adv. Water Resour. 50, 79–90. https://doi.org/10.1016/j.advwatres.2012.07.023.
Fisher, J.B., Melton, F., Middleton, E., Hain, C., Anderson, M., Allen, R., McCabe, M.F., Hook, S., Baldocchi, D., Townsend, P.A., Kilic, A., Tu, K., Miralles, D.D., Perret, J., Lagouarde, J.P., Waliser, D., Purdy, A.J., French, A., Schimel, D., Wood, E.F., 2017. The future of evapotranspiration: global requirements for ecosystem functioning, carbon and climate feedbacks, agricultural management, and water resources. Water Resour. Res. 53 (4), 2618–2626. https://doi.org/10.1002/2016WR020175.
Foken, T., Aubinet, M., Finnigan, J.J., Leclerc, M.Y., Mauder, M., Paw U, K.T., 2011. Results of a panel discussion about the energy balance closure correction for trace gases. Bull. Am. Meteorol. Soc. 92 (4), 13–18. https://doi.org/10.1175/2011BAMS3130.1.
Forstner, V., Groh, J., Vremec, M., Herndl, M., Vereecken, H., Gerke, H.H., Birk, S., Pütz, T., 2021. Supplementrary Response of water fluxes and biomass production to climate change in permanent grassland soil ecosystems. Hydrol. Earth Syst. Sci. 25 (12), 6087–6106. https://doi.org/10.5194/hess-25-6087-2021.
Fraenkel, J.R., Wallen, N.E., 1990. How to Design and Evaluate Research in Education. ERIC.
Franssen, H.J.H., Stöckli, R., Lehner, I., Rotenberg, E., Seneviratne, S.I., 2010. Energy balance closure of eddy-covariance data : a multisite analysis for European FLUXNET stations. Agric. For. Meteorol. https://doi.org/10.1016/j.agrformet.2010.08.005.
Fu, J., Gasche, R., Wang, N., Lu, H., Butterbach-Bahl, K., Kiese, R., 2017. Impacts of climate and management on water balance and nitrogen leaching from montane grassland soils of S-Germany. Environ. Pollut. 229, 119–131. https://doi.org/10.1016/j.envpol.2017.05.071.
Fu, J., Gasche, R., Wang, N., Lu, H., Butterbach-Bahl, K., Kiese, R., 2019. Dissolved organic carbon leaching from montane grasslands under contrasting climate, soil and management conditions. Biogeochemistry 145 (1–2), 47–61. https://doi.org/10.1007/s10533-019-00589-y.
Gebler, S., Hendricks Franssen, H.J., Pütz, T., Post, H., Schmidt, M., Vereecken, H., 2015. Actual evapotranspiration and precipitation measured by lysimeters: a comparison with eddy covariance and tipping bucket. Hydrol. Earth Syst. Sci. 19 (5), 2145–2161. https://doi.org/10.5194/hess-19-2145-2015.
Goss, M.J., Ehlers, W., 2009. The role of lysimeters in the development of our understanding of soil water and nutrient dynamics in ecosystems. Soil Use Manag. 25 (3), 213–223. https://doi.org/10.1111/j.1475-2743.2009.00230.x.
Graf, A., Bogena, H.R., Drüe, C., Hardelauf, H., Pütz, T., 2014. Spatiotemporal relations between water budget components and soil water content in a forested tributary catchment alexander. Water Resour. Res. 5375–5377. https://doi.org/10.1002/2013WR014979.Reply.
Graf, A., Klosterhalfen, A., Arriga, N., Bernhofer, C., Bogena, H., Bornet, F., Brüggemann, N., Brümmer, C., Buchmann, N., Chi, J., Chipeaux, C., Cremonese, E., Cuntz, M., Dušek, J., El-Madany, T.S., Fares, S., Fischer, M., Foltýnová, L., Gharun, M., Vereecken, H., 2020. Altered energy partitioning across terrestrial ecosystems in the European drought year 2018: energy partitioning in the drought 2018. Philos. Trans. R. Soc. B Biol. Sci. 375 (1810). https://doi.org/10.1098/rstb.2019.0524.
Grinsted, A., Moore, J.C., Jevrejeva, S., 2004. Application of the cross wavelet transform and wavelet coherence to geophysical time series. Nonlinear Process. Geophys. 11 (4), 515–533. https://doi.org/10.5194/npg-11-515-2004.
Groh, J., Diamantopoulos, E., Duan, X., Ewert, F., Heinlein, F., Herbst, M., Holbak, M., Kamali, B., Kersebaum, K.C., Kuhnert, M., Nendel, C., Priesack, E., Steidl, J., Sommer, M., Pütz, T., Vanderborght, J., Vereecken, H., Wallor, E., Weber, T.K.D., Gerke, H.H., 2022. Same soil, different climate: crop model intercomparison on translocated lysimeters. Vadose Zone J. 21 (4), 1–25. https://doi.org/10.1002/vzj2.20202.
Groh, J., Pütz, T., Gerke, H.H., Vanderborght, J., Vereecken, H., 2019. Quantification and prediction of nighttime evapotranspiration for two distinct grassland ecosystems. Water Resour. Res. 55 (4), 2961–2975. https://doi.org/10.1029/2018WR024072.
Groh, J., Slawitsch, V., Herndl, M., Graf, A., Vereecken, H., Pütz, T., 2018. Determining dew and hoar frost formation for a low mountain range and alpine grassland site by weighable lysimeter. J. Hydrol. 563 (November 2017), 372–381. https://doi.org/10.1016/j.jhydrol.2018.06.009.
Groh, J., Vanderborght, J., Pütz, T., Vereecken, H., 2016. How to control the lysimeter bottom boundary to investigate the effect of climate change on soil processes? Vadose Zone J. 15 (7). https://doi.org/10.2136/vzj2015.08.0113 vzj2015.08.0113.
Grumm, R.H., Hart, R., 2001. Standardized anomalies applied to significant cold season weather events: preliminary findings. Weather Forecast. 736–754.
Han, Q., Wang, T., Wang, L., Smettem, K., Mai, M., Chen, X., 2021. Comparison of nighttime with daytime evapotranspiration responses to environmental controls across temporal scales along a climate gradient. Water Resour. Res. 57 (7), 1–18. https://doi.org/10.1029/2021WR029638.
Hanson R.L. (1991). Evapotranspiration and droughts. National Water Summary 1988–89: Hydrologic Events and Floods and Droughts (US Geological Survey Water-Supply Paper 2375), 99–104.
Hirschi, M., Michel, D., Lehner, I., Seneviratne, S.I., 2017. A site-level comparison of lysimeter and eddy covariance flux measurements of evapotranspiration. Hydrol. Earth Syst. Sci. 21 (3), 1809–1825. https://doi.org/10.5194/hess-21-1809-2017.
Hollinger, D.Y., Richardson, A.D., 2005. Uncertainty in eddy covariance measurements and its application to physiological models. Tree Physiol. 25 (7), 873–885. https://doi.org/10.1093/treephys/25.7.873.
Hu, W., Si, B., 2021. Technical Note: improved partial wavelet coherency for understanding scale-specific and localized bivariate relationships in geosciences. Hydrol. Earth Syst. Sci. 25 (1), 321–331. https://doi.org/10.5194/hess-25-321-2021.
Hu, W., Si, B.C., 2016. Technical note: multiple wavelet coherence for untangling scale-specific and localized multivariate relationships in geosciences. Hydrol. Earth Syst. Sci. 20 (8), 3183–3191. https://doi.org/10.5194/hess-20-3183-2016.
Hu, W., Si, B.C., Biswas, A., Chau, H.W., 2017. Temporally stable patterns but seasonal dependent controls of soil water content: evidence from wavelet analyses. Hydrol. Process. 31 (21), 3697–3707. https://doi.org/10.1002/hyp.11289.
Kessomkiat, W., Franssen, H.J.H., Graf, A., Vereecken, H., 2013. Estimating random errors of eddy covariance data: an extended two-tower approach. Agric. For. Meteorol. 171–172, 203–219. https://doi.org/10.1016/j.agrformet.2012.11.019.
Kiese, R., Fersch, B., Baessler, C., Brosy, C., Butterbach-Bahl, K., Chwala, C., Dannenmann, M., Fu, J., Gasche, R., Grote, R., Jahn, C., Klatt, J., Kunstmann, H., Mauder, M., Rödiger, T., Smiatek, G., Soltani, M., Steinbrecher, R., Völksch, I., Schmid, H.P., 2018. The TERENO pre-alpine observatory: integrating meteorological, hydrological, and biogeochemical measurements and modeling. Vadose Zone J. 17 (1), 180060. https://doi.org/10.2136/vzj2018.03.0060.
Kim, D., Choi, M., Chun, J.A., 2022. Linking the complementary evaporation relationship with the Budyko framework for ungauged areas in Australia. Hydrol. Earth Syst. Sci. 26 (23), 5955–5969. https://doi.org/10.5194/hess-26-5955-2022.
Kohfahl, C., Molano-Leno, L., Martínez, G., Vanderlinden, K., Guardiola-Albert, C., Moreno, L., 2019. Determining groundwater recharge and vapor flow in dune sediments using a weighable precision meteo lysimeter. Sci. Total Environ. 656, 550–557. https://doi.org/10.1016/j.scitotenv.2018.11.415.
Kool, D., Agam, N., Lazarovitch, N., Heitman, J.L., Sauer, T.J., Ben-Gal, A., 2014. A review of approaches for evapotranspiration partitioning. Agric. For. Meteorol. 184, 56–70. https://doi.org/10.1016/j.agrformet.2013.09.003.
Korres, W., Reichenau, T.G., Fiener, P., Koyama, C.N., Bogena, H.R., Cornelissen, T., Baatz, R., Herbst, M., Diekkrüger, B., Vereecken, H., Schneider, K., 2015. Spatio-temporal soil moisture patterns - A meta-analysis using plot to catchment scale data. J. Hydrol. 520, 326–341. https://doi.org/10.1016/j.jhydrol.2014.11.042.
Labat, D., 2005. Recent advances in wavelet analyses: part 1. A review of concepts. J. Hydrol. 314 (1), 275–288. https://doi.org/10.1016/j.jhydrol.2005.04.003.
Levy, P., Clement, R., Cowan, N., Keane, B., Myrgiotis, V., van Oijen, M., Smallman, T.L., Toet, S., Williams, M., 2022. Challenges in scaling up greenhouse gas fluxes: experience from the UK greenhouse gas emissions and feedbacks program. J. Geophys. Res. Biogeosciences 127 (5), 1–22. https://doi.org/10.1029/2021JG006743.
Li, W., Hendricks Franssen, H.J., Brunner, P., Li, Z., Wang, Z., Wang, Y., Wang, W., 2022. The role of soil texture on diurnal and seasonal cycles of potential evaporation over saturated bare soils – Lysimeter studies. J. Hydrol. 613 (2021). https://doi.org/10.1016/j.jhydrol.2022.128194.
Liu, Q., Hao, Y., Stebler, E., Tanaka, N., Zou, C.B., 2017. Impact of plant functional types on coherence between precipitation and soil moisture: a wavelet analysis. Geophys. Res. Lett. 44 (24). https://doi.org/10.1002/2017GL075542, 12,197-12,207.
Maraun, D., Kurths, J., 2004. Cross wavelet analysis: significance testing and pitfalls D. Nonlinear Process. Geophys. 11 (3), 363–370. https://doi.org/10.5194/npg-11-363-2004.
Mauder, M., Cuntz, M., Drüe, C., Graf, A., Rebmann, C., Schmid, H.P., Schmidt, M., Steinbrecher, R., 2013. A strategy for quality and uncertainty assessment of long-term eddy-covariance measurements. Agric. For. Meteorol. 169, 122–135. https://doi.org/10.1016/j.agrformet.2012.09.006.
Mauder, M., Foken, T., 2011. Documentation and instruction manual of the eddy-covariance software package TK3. Arbeitsergebnisse 3 (46), 60. ISSN 1614-8916. http://nbn-resolving.de/urn/resolver.pl?urn:nbn:de:bvb:703-opus-8665%5Cnhttp://opus4.kobv.de/opus4-ubbayreuth/frontdoor/index/index/docId/681.
Mauder, M., Foken, T., Cuxart, J., 2020. Surface-energy-balance closure over land: a review. In: Boundary-Layer Meteorology, 177. Springer, the Netherlands. https://doi.org/10.1007/s10546-020-00529-6.
Mauder, M., Genzel, S., Fu, J., Kiese, R., Soltani, M., Steinbrecher, R., Zeeman, M., Banerjee, T., De Roo, F., Kunstmann, H., 2018. Evaluation of energy balance closure adjustment methods by independent evapotranspiration estimates from lysimeters and hydrological simulations. Hydrol. Process. 32 (1), 39–50. https://doi.org/10.1002/hyp.11397.

Mueller, B., Seneviratne, S.I., Jimenez, C., Corti, T., Hirschi, M., Balsamo, G., Ciais, P., Dirmeyer, P., Fisher, J.B., Guo, Z., Jung, M., Maignan, F., McCabe, M.F., Reichle, R., Reichstein, M., Rodell, M., Sheffield, J., Teuling, A.J., Wang, K., Zhang, Y., 2011. Evaluation of global observations-based evapotranspiration datasets and IPCC AR4 simulations. Geophys. Res. Lett. 38 (6), 1–7. https://doi.org/10.1029/2010GL046230.

Negm, A., Jabro, J., Provenzano, G., 2017. Assessing the suitability of American National Aeronautics and Space Administration (NASA) agro-climatology archive to predict daily meteorological variables and reference evapotranspiration in Sicily, Italy. Agric. For. Meteorol. 244–245 (October 2016), 111–121. https://doi.org/10.1016/j.agrformet.2017.05.022.

Paulus S.J., Orth R., Lee S., Hildebrandt A., Jung M., Nelson J.A., El-madany S., Carrara A., Moreno G., Mauder M., Groh J., & Graf A. (2024). Interpretability of Negative Latent Heat Fluxes from Eddy Covariance Measurements in Dry Conditions. 2051–2085.

Paulus, S.J., El-Madany, T.S., Orth, R., Hildebrandt, A., Wutzler, T., Carrara, A., Moreno, G., Perez-Priego, O., Kolle, O., Reichstein, M., Migliavacca, M., 2022. Resolving seasonal and diel dynamics of non-rainfall water inputs in a Mediterranean ecosystem using lysimeters. Hydrol. Earth Syst. Sci. 26 (23), 6263–6287. https://doi.org/10.5194/hess-26-6263-2022.

Peters, A., Nehls, T., Schonsky, H., Wessolek, G., 2014. Separating precipitation and evapotranspiration from noise - A new filter routine for high-resolution lysimeter data. Hydrol. Earth Syst. Sci. 18 (3), 1189–1198. https://doi.org/10.5194/hess-18-1189-2014.

Peters, A., Groh, J., Schrader, F., Durner, W., Vereecken, H., Pütz, T., 2017. Towards an unbiased filter routine to determine precipitation and evapotranspiration from high precision lysimeter measurements. J. Hydrol. 549, 731–740. https://doi.org/10.1016/j.jhydrol.2017.04.015.

Post, H., Hendricks Franssen, H.J., Graf, A., Schmidt, M., Vereecken, H., 2015. Uncertainty analysis of eddy covariance CO2 flux measurements for different EC tower distances using an extended two-tower approach. Biogeosciences 12 (4), 1205–1221. https://doi.org/10.5194/bg-12-1205-2015.

Pütz, T., Kiese, R., Wollschläger, U., Groh, J., Rupp, H., Zacharias, S., Priesack, E., Gerke, H.H., Gasche, R., Bens, O., Borg, E., Baessler, C., Kaiser, K., Herbrich, M., Munch, J.C., Sommer, M., Vogel, H.J., Vanderborght, J., Vereecken, H., 2016. TERENO-SOILCan: a lysimeter-network in Germany observing soil processes and plant diversity influenced by climate change. Environ. Earth Sci. 75 (18), 1242. https://doi.org/10.1007/s12665-016-6031-5.

Rabbel I. (2018). Analyzing Feedbacks in a Forest Soil-Vegetation-Atmosphere System.

Rahmati, M., Groh, J., Graf, A., Pütz, T., Vanderborght, J., Vereecken, H., 2020. On the impact of increasing drought on the relationship between soil water content and evapotranspiration of a grassland. Vadose Zone J. 19 (1), 1–20. https://doi.org/10.1002/vzj2.20029.

Rodriguez-Iturbe, I., 2000. Ecohydrology: a hydrologic perspective of climate-soil-vegetation dynamics. Water Resour. Res. https://doi.org/10.1029/1999WR900210.

Sánchez, J.M., López-Urrea, R., Valentín, F., Caselles, V., Galve, J.M., 2019. Lysimeter assessment of the simplified two-source energy balance model and eddy covariance system to estimate vineyard evapotranspiration. Agric. For. Meteorol. 274 (September 2018), 172–183. https://doi.org/10.1016/j.agrformet.2019.05.006.

Schneider, J., Groh, J., Pütz, T., Helmig, R., Rothfuss, Y., Vereecken, H., Vanderborght, J., 2021. Prediction of soil evaporation measured with weighable lysimeters using the FAO Penman–Monteith method in combination with Richards' equation. Vadose Zone J. 20 (1), 1–20. https://doi.org/10.1002/vzj2.20102.

Schnepper, T., Groh, J., Gerke, H.H., Reichert, B., Pütz, T., 2023. Evaluation of precipitation measurement methods using data from a precision lysimeter network. Hydrol. Earth Syst. Sci. 27, 3265–3292. https://doi.org/10.5194/hess-27-3265-2023.

Schrader, F., Durner, W., Fank, J., Gebler, S., Pütz, T., Hannes, M., Wollschläger, U., 2013. Estimating precipitation and actual evapotranspiration from precision lysimeter measurements. Procedia Environ. Sci. 19, 543–552. https://doi.org/10.1016/j.proenv.2013.06.061.

Seneviratne, S.I., Lehner, I., Gurtz, J., Teuling, A.J., Lang, H., Moser, U., Grebner, D., Menzel, L., Schroff, K., Vitvar, T., Zappa, M., 2012. Swiss prealpine Rietholzbach research catchment and lysimeter: 32 year time series and 2003 drought event. Water Resour. Res. 48 (6), 1–20. https://doi.org/10.1029/2011WR011749.

Straaten, A., Weber, S., 2021. Measurement report: three years of size-resolved eddy-covariance particle number flux measurements in an urban environment. Atmos. Chem. Phys. 21 (24), 18707–18726. https://doi.org/10.5194/acp-21-18707-2021.

Su, L., Miao, C., Duan, Q., Lei, X., Li, H., 2019. Multiple-wavelet coherence of world's large rivers with meteorological factors and ocean signals. J. Geophys. Res. Atmos. 124 (9), 4932–4954. https://doi.org/10.1029/2018JD029842.

Tadesse, T., Senay, G.B., Berhan, G., Regassa, T., 2015. International journal of applied earth observation and geoinformation evaluating a satellite-based seasonal evapotranspiration product and identifying its relationship with other satellite-derived products and crop yield : a case study for Ethiopia. Int. J. Appl. Earth Obs. Geoinf. 40, 39–54. https://doi.org/10.1016/j.jag.2015.03.006.

Teuling, A.J., 2018. A forest evapotranspiration paradox investigated using lysimeter data. Vadose Zone J. 17 (1), 1–7. https://doi.org/10.2136/vzj2017.01.0031.

Torrence, C., Compo, G.P., 1998. A practical guide to wavelet analysis. Bull. Am. Meteorol. Soc. 79 (1), 61–78.

Tran B., Van Der Kwast J., Seyoum S., Uijlenhoet R., Jewitt G., & Mul M. (2023). Uncertainty assessment of satellite remote sensing-based evapotranspiration estimates: a systematic review of methods and gaps. EGUsphere Preprint Repository, 1–40. 10.5194/egusphere-2023-725.

Trigo, I.F., de Bruin, H., Beyrich, F., Bosveld, F.C., Gavilán, P., Groh, J., López-Urrea, R., 2018. Validation of reference evapotranspiration from Meteosat Second Generation (MSG) observations. Agric. For. Meteorol. 259 (September 2017), 271–285. https://doi.org/10.1016/j.agrformet.2018.05.008.

Twine, T.E., Kustas, W.P., Norman, J.M., Cook, D.R., Houser, P.R., Meyers, T.P., Prueger, J.H., Starks, P.J., Wesely, M.L., 2000. Correcting eddy-covariance flux underestimates over a grassland. Agric. For. Meteorol. 103 (3), 279–300. https://doi.org/10.1016/S0168-1923(00)00123-4.

Unold, G.V, Fank, J., 2008. Modular design of field lysimeters for specific application needs. Water Air Soil Pollut: Focus 233–242. https://doi.org/10.1007/s11267-007-9172-4.

Widmoser, P., Michel, D., 2021. Partial energy balance closure of eddy covariance evaporation measurements using concurrent lysimeter observations over grassland. Hydrol. Earth Syst. Sci. 25 (3), 1151–1163. https://doi.org/10.5194/hess-25-1151-2021.

Wilson, K.B., Hanson, P.J., Mulholland, P.J., Baldocchi, D.D., Wullschleger, S.D., 2001. A comparison of methods for determining forest evapotranspiration and its components: sap-flow, soil water budget, eddy covariance and catchment water balance. Agric. For. Meteorol. 106 (2), 153–168. https://doi.org/10.1016/S0168-1923(00)00199-4.

Wu, D., Di, C., Wang, T., Wang, L., Chen, X., 2021. Characterization of the coherence between soil moisture and precipitation at regional scales. J. Geophys. Res. Atmos. 126 (8), 1–14. https://doi.org/10.1029/2020JD034340.

Zacharias, S., Bogena, H., Samaniego, L., Mauder, M., Fuß, R., Pütz, T., Frenzel, M., Schwank, M., Baessler, C., Butterbach-Bahl, K., 2011. A network of terrestrial environmental observatories in Germany. Vadose Zone J. 10 (3), 955–973.

Zeeman, M.J., Mauder, M., Steinbrecher, R., Heidbach, K., Eckart, E., Schmid, H.P., 2017. Reduced snow cover affects productivity of upland temperate grasslands. Agric. For. Meteorol. 232, 514–526. https://doi.org/10.1016/j.agrformet.2016.09.002.

Zhang, W., Jung, M., Migliavacca, M., Poyatos, R., Miralles, D., El-Madany, T.S., Galvagno, M., Carrara, A., Arriga, N., Ibrom, A., Mammarella, I., Papale, D., Cleverly, J., Liddell, M.J., Wohlfahrt, G., Markwitz, C., Mauder, M., Paul-Limoges, E., Schmidt, M., Nelson, J.A., 2022. The effect of relative humidity on eddy covariance latent heat flux measurements and its implication for partitioning into transpiration and evaporation. Agric For Meteorol, January. https://doi.org/10.2139/ssrn.4106267.

Zhang, Z., Tian, F., Hu, H., Yang, P., 2014. A comparison of methods for determining field evapotranspiration: photosynthesis system, sap flow, and eddy covariance. Hydrol. Earth Syst. Sci. 18 (3), 1053–1072. https://doi.org/10.5194/hess-18-1053-2014.

Zhu, S., Olde, L., Lewis, K., Quaife, T., Cardenas, L., Loick, N., Xu, J., Hill, T., 2023. Eddy covariance fluxes over managed ecosystems extrapolated to field scales at fine spatial resolutions. Agric. For. Meteorol. 342, 109675. https://doi.org/10.1016/J.AGRFORMET.2023.109675.